NASA TECHNICAL NOTE

NASA TN D-7190

NASA TN D-7190

EVALUATION OF COMPRESSIBLE-FLOW PRESTON TUBE CALIBRATIONS

by Jerry M. Allen

Langley Research Center
Hampton, Va. 23365

NATIONAL AERONAUTICS AND SPACE ADMINISTRATION • WASHINGTON, D. C. • MAY 1973

1. Report No.	2. Government Accession No.	3. Recipient's Catalog No.
NASA TN D-7190		

4. Title and Subtitle	5. Report Date
EVALUATION OF COMPRESSIBLE-FLOW PRESTON TUBE CALIBRATIONS	May 1973
	6. Performing Organization Code

7. Author(s)	8. Performing Organization Report No.
Jerry M. Allen	L-8733
	10. Work Unit No.
9. Performing Organization Name and Address	760-65-01-01
NASA Langley Research Center Hampton, Va. 23665	11. Contract or Grant No.
	13. Type of Report and Period Covered
12. Sponsoring Agency Name and Address	Technical Note
National Aeronautics and Space Administration Washington, D.C. 20546	14. Sponsoring Agency Code

15. Supplementary Notes

16. Abstract

An experimental and analytical study has been made of the accuracy of various Preston tube calibration equations to determine local skin friction in two-dimensional supersonic and low-hypersonic flows. Experimental Preston tube calibration data from the present and previous studies were used to evaluate the calibration equations. The maximum value of the calibration parameters of the present data is more than an order of magnitude larger than that previously obtained; thereby, the evaluation of the various calibration equations is facilitated.

The Preston tube technique was found to be very inaccurate in the low range of the calibration parameters. Above this range, there was a steady increase in accuracy with increasing values of the calibration parameters. No critical maximum tube diameter was found even with tubes about twice as large as the theoretical maximum allowable diameter.

Of the two forms of the calibration equation previously existing, the logarithmic laws gave more accurate results than the power laws over an extended range of the calibration parameters in supersonic adiabatic flow. Major deficiencies in the calibration equations were found to exist for the Fenter-Stalmach equation under low-hypersonic cold-wall conditions, and for the Hopkins-Keener equation under high-supersonic large-tube-diameter conditions. The second-order least-squares calibration equation developed in this paper gave the best overall results of the calibration equations evaluated.

17. Key Words (Suggested by Author(s))	18. Distribution Statement
Preston tube calibrations Supersonic flow Boundary layer Skin-friction balance	Unclassified – Unlimited

19. Security Classif. (of this report)	20. Security Classif. (of this page)	21. No. of Pages	22. Price*
Unclassified	Unclassified	67	$3.00

*For sale by the National Technical Information Service, Springfield, Virginia 22151

CONTENTS

EVALUATION OF COMPRESSIBLE-FLOW PRESTON TUBE CALIBRATIONS

By Jerry M. Allen
Langley Research Center

SUMMARY

An experimental and analytical study has been made of the accuracy of various Preston tube calibration equations to determine local skin friction in two-dimensional supersonic and low-hypersonic flows. Experimental Preston tube calibration data from the present and previous studies were used to evaluate the calibration equations. The maximum value of the calibration parameters of the present data is more than an order of magnitude larger than that previously obtained; thereby, the evaluation of the various calibration equations is facilitated.

The Preston tube technique was found to be very inaccurate in the low range of the calibration parameters. Above this range, there was a steady increase in accuracy with increasing values of the calibration parameters. No critical maximum tube diameter was found even with tubes about twice as large as the theoretical maximum allowable diameter.

Of the two forms of the calibration equation previously existing, the logarithmic laws gave more accurate results than the power laws over an extended range of the calibration parameters in supersonic adiabatic flow. Major deficiencies in the calibration equations were found to exist for the Fenter-Stalmach equation under low-hypersonic cold-wall conditions, and for the Hopkins-Keener equation under high-supersonic large-tube-diameter conditions. The second-order least-squares calibration equation developed in this paper gave the best overall results of the calibration equations evaluated.

INTRODUCTION

Studies by many investigators have for some time established that the surface pitot tube can be used to measure local turbulent skin friction. The introduction of reference 1 contains a thorough chronological review of previous studies in this field. For circular surface pitot tubes the term "Preston tube" is used, after the author of reference 2. References 1 to 5 contain important contributions to the field of Preston tubes in adiabatic two-dimensional turbulent flow.

Basically, the Preston tube technique consists of bringing the circular tube into contact with the test surface at the location where local skin friction is desired, measuring the pitot pressure sensed by the tube, and combining this pressure with local free-stream conditions and tube diameter to calculate local skin friction from an existing calibration equation. The main advantages of the Preston tube over other skin-friction measuring devices are its sturdiness, simplicity of use, and the fact that calibration of individual tubes is not required.

In previous experiments in compressible flow (refs. 1 and 3), it was found that the data from all Reynolds numbers, Mach numbers, and tube diameters tested collapsed onto a single curve when the appropriate calibration parameters were used. The calibrations were thus reported to be independent of Mach and Reynolds numbers and tube diameter and can be used by the experimenter without the need of calibrating his tubes.

Patel (ref. 5) developed an incompressible flow calibration which he reports to be an improvement over Preston's original calibration. A compressible-flow calibration based on Patel's law is developed in this paper. Also, least-squares curve fits to experimental data are performed to obtain a calibration equation which is the best fit to the data

These new calibrations and existing compressible-flow calibrations are evaluated in this paper for their accuracy in determining local skin friction. The evaluations are performed by using existing supersonic adiabatic-wall Preston tube data (refs. 1 and 3) and new data obtained in this study which includes results at larger Mach numbers and Reynolds numbers based on tube diameter than previously existed. The larger values of these parameters permit an easier evaluation of the various calibration equations since they tend to diverge for these conditions. The following table illustrates the extensions in these two parameters provided by the data of the present study:

Authors	Reference	Mach number range	Reynolds number based on tube diameter range
Fenter and Stalmach	3	1.7 to 3.7	2.7×10^3 to 65×10^3
Hopkins and Keener	1	2.4 to 3.4	2.4×10^3 to 51×10^3
Present study	---	2.0 to 4.6	2.5×10^3 to 800×10^3

The large value of Reynolds number based on tube diameter obtained in the present study is the result of testing a wide range of tube diameters. Analytical studies in the past (refs. 1, 3, and 6) have estimated the range of tube sizes which should give valid results. The following table shows that in the previous investigations, only small ranges of tube sizes were used:

Authors	Reference	External diameters used, mm	Largest tube / Smallest tube	Size range theoretically usable, mm
Fenter and Stalmach	3	0.31 to 1.65	5.3	0.2 to 2.0
Hopkins and Keener	1	1.55 to 6.35	4.1	0.7 to 45.0
Present study	---	1.27 to 48.26	38.0	0.4 to 46.5

Each of the previous studies tested four tube sizes and indicated that valid results were obtained with each. Neither study, therefore, was designed to show the effect of tube size on the calibration results. The wide range of sizes used in this study allowed such effects to be investigated.

Finally, the ability of the various calibration equations to determine local skin friction under low-hypersonic cold-wall conditions is evaluated by comparing the equations with the calibration data of reference 7.

SYMBOLS

U.S. Customary Units were employed for the experimental measurements in this study, but the International System of Units (SI) is used herein to report the results.

A skin-friction-balance floating-element area

C_f average skin-friction coefficient, $\frac{1}{x}\int_0^x c_f \, dx$

c_f local skin-friction coefficient, τ_w/q_e

D Preston tube external diameter

d Preston tube internal diameter

F_1, F_2, F_3, F_4, F_5 Preston tube calibration parameters (see eqs. (20))

i index

M Mach number

N power-law velocity profile exponent

p	static pressure
p_t	stagnation pressure
q	dynamic pressure, $\frac{1}{2}\rho u^2$
R	unit Reynolds number, $\frac{\rho u}{\mu}$
R_D	local free-stream Reynolds number based on D, $\frac{\rho_e u_e D}{\mu_e}$
R_θ	local free-stream Reynolds number based on θ, $\frac{\rho_e u_e \theta}{\mu_e}$
S	wall shearing force
T	static temperature
T_t	stagnation temperature
T'	reference temperature (see eq. (31))
u	velocity in x-direction
u_τ	friction velocity, $\sqrt{\frac{\tau_w}{\rho}}$
x	streamwise coordinate
y	normal coordinate
γ	ratio of specific heats (=1.4 for air)
δ	boundary-layer total thickness
δ^*	boundary-layer displacement thickness (see eq. (8))
θ	boundary-layer momentum thickness (see eq. (7))
μ	viscosity
ν	kinematic viscosity, $\frac{\mu}{\rho}$

ρ density

τ shearing stress

Subscripts:

aw adiabatic-wall value

c calculated from Preston tube calibration

e boundary-layer edge value

m measured

max calculated maximum value

min calculated minimum value

w wall value

∞ free-stream value

Primes denote fluid properties evaluated at reference temperature T'.

APPARATUS AND TESTS

Wind Tunnels

The Mach number 2.3 and 4.6 data used in this study were obtained in the high-speed test section of the Langley Unitary Plan wind tunnel, which is described in reference 8. This variable-pressure, continuous-flow tunnel has a two-dimensional asymmetric sliding-block nozzle that permits a continuous variation in the test-section Mach number from about 2.3 to 4.6. The normal operating stagnation temperature is between 66° C and 79° C. The test section is approximately 1.22 meters wide by 1.22 meters high by 2.13 meters long.

The Mach number 2.0 data were obtained as a part of the pitot-tube displacement study reported in reference 9. This test was conducted in the Langley 4- by 4-foot supersonic pressure tunnel which is also described in reference 8. This facility is a rectangular, closed test section, single-return wind tunnel with provisions for control of pressure, temperature, and humidity of the enclosed air. Two flexible walls of the two-dimensional nozzle can be adjusted to give Mach numbers from 1.4 to 2.6. The normal operating temperature is about 43° C. The test section is about the same size as the test section of the Unitary Plan wind tunnel.

Test Stations

Both tunnels, as described earlier, have two-dimensional nozzles. The top and bottom walls are contoured to produce the supersonic flow. The sidewalls, used as the test surfaces, are flat from the nozzle throat to the downstream edge of the test section. In both tunnels the permanent model support mechanism was located downstream of the survey station and was traversed to the opposite side of the test section to insure that no flow disturbances originating from the mechanism could affect the results of this study.

In the Unitary Plan wind tunnel the turbulent boundary layer was surveyed on the sidewall center line about midway of the test section. The boundary layer at the survey station was about 12 cm to 16 cm thick, depending on the test conditions. The equivalent flat-plate length (that is, length of turbulent flat-plate flow at the same free-stream conditions of the survey station needed to produce the same boundary layer) to the survey station was about 6.8 to 8.7 meters.

In the 4- by 4-foot tunnel, the survey station was located on the sidewall center line in the downstream part of the test section. This survey station was located about 5 meter from the nozzle throat and provided a turbulent boundary layer about 7 cm thick. The equivalent flat-plate length was about 4.5 meters.

Instrumentation

The tunnel sidewall boundary layer was surveyed with a small, flattened boundary-layer pitot tube. Preston tube measurements were made with 8 tubes ranging in outside diameter from about 1.3 mm to 48 mm. Tube sketches and dimensions can be found in figure 1.

The tubes were mounted on a shaft which ran through the tunnel sidewall. Tube position normal to the wall was controlled manually from outside the tunnel by a traversing mechanism connected to the tube shaft. The surface location was determined by electrical contact between the wall and the tube; and the distance above the test surface was calculated from the surface contact point and a dial indicator connected to the tube shaft.

The pressures from these tubes were sensed by three pressure transducers, the ranges of which were 0 to 0.34, 0 to 0.68, and 0 to 1.02 atmospheres. (One atmosphere equals 1.013×10^5 N/m^2.) In this manner the gage having the smallest possible range could be used for maximum accuracy. Tunnel stagnation pressures were measured by precision automatic indicating mercury manometers.

Local shearing forces were measured by a floating-element skin-friction balance mounted so that the sensing element was flush with the test surface at the survey station. This balance is a self-nulling type of instrument whose output voltage is directly propor-

tioned to the skin-friction force on the sensing element. The balance is commercially available and is described in detail in reference 10.

Tests and Procedures

The nominal free-stream flow conditions of all the data obtained in this study are presented in table I. About 30 minutes was allowed between the establishment of supersonic flow and the recording of experimental data to insure that pressure and temperature conditions in the test section had reached equilibrium. The test-section wall temperatures under these equilibrium conditions were within a few degrees of the calculated adiabatic-wall temperatures; hence, this study was assumed to be conducted under adiabatic-wall conditions.

Boundary-layer surveys were made at the test station at each of the free-stream flow conditions by using the flattened tube. The test procedure consisted of bringing the tube in contact with the tunnel wall, as determined by the contact light, and then moving the tube away from the wall in small increments and recording the data.

Preston tube measurements were made at the same test station that the boundary-layer surveys were made. These measurements were obtained with each of the 8 circular tubes in contact with the test surface. These tubes, as can be seen from the sketches in figure 1, were double-ended; that is, two tubes were mounted back-to-back on a single shaft. In this configuration, data from two tubes could be recorded without the necessity of a tunnel shutdown, tube change, and subsequent tunnel restart. This procedure allowed the cutting of tunnel running time approximately in half. Insulating tape was applied to the tunnel wall in the area immediately downstream of the shaft to insure that the contact light would be activated only by the upstream tube touching the wall.

The procedure for recording data with these double-ended tubes was as follows: (1) with the tubes in contact with the test surface, data were recorded for the tube facing upstream, (2) the tube was then traversed away from the test surface, and the entire assembly was rotated 180° so that the second tube pointed upstream, and (3) the tubes were again brought in contact with the test surface, and data from the second tube were recorded.

After the pitot tube data had been recorded, a new tunnel sidewall insert was installed to house the skin-friction balance. The center line of the balance was located a few centimeters downstream of the location where the tip of the tubes had been. This difference in x meant that for the same free-stream test conditions, the balance data were recorded at a slightly higher Reynolds number than the pitot pressure data. It was estimated that the effective length Reynolds number increased about 0.2 percent, which would result in an error in c_f of about 0.03 percent. Since the error was so small, no corrections were applied to the measured skin friction for this effect.

DATA REDUCTION

Mach Number

The measured pitot tube pressures outside the boundary layer $p_{t,m,e}$ and the measured tunnel stagnation pressures $p_{t,\infty}$ were used to calculate the local free-stream Mach numbers by the normal-shock relation

$$\frac{p_{t,m,e}}{p_{t,\infty}} = \left[\frac{(\gamma + 1)M_e^2}{(\gamma - 1)M_e^2 + 2}\right]^{\frac{\gamma}{\gamma-1}} \left(\frac{\gamma + 1}{2\gamma M_e^2 - \gamma + 1}\right)^{\frac{1}{\gamma-1}} \tag{1}$$

These Mach numbers and $p_{t,m,e}$ values were then used to calculate the static pressure at the boundary-layer edge p_e from the Rayleigh pitot formula

$$\frac{p_{t,m,e}}{p_e} = \left[\frac{(\gamma + 1)M_e^2}{2}\right]^{\frac{\gamma}{\gamma-1}} \left(\frac{\gamma + 1}{2\gamma M_e^2 - \gamma + 1}\right)^{\frac{1}{\gamma-1}} \tag{2}$$

The static pressure was then assumed to be constant through the boundary layer and equal to the calculated edge values. The Mach number distributions through the boundary layer were then calculated from the measured $p_{t,m}$ and calculated p_e values. If $p_{t,m}/p_e$ was greater than 1.893, the supersonic Mach numbers were calculated by equation (2) in which local conditions replace the boundary-layer edge conditions. If $p_{t,m}/p_e$ was less than 1.893, the subsonic Mach numbers were calculated from the isentropic flow equation

$$\frac{p_{t,m}}{p_e} = \left(1 + \frac{\gamma - 1}{2} M^2\right)^{\frac{\gamma}{\gamma-1}} \tag{3}$$

Velocity Ratio

Velocity ratios are related to Mach number and temperature by

$$\frac{u}{u_e} = \frac{M}{M_e}\sqrt{\frac{T}{T_t}}\sqrt{\frac{T_{t,e}}{T_e}}\sqrt{\frac{T_t}{T_{t,e}}} \tag{4}$$

where

$$\left.\begin{aligned} \frac{T_t}{T} &= 1 + \frac{\gamma - 1}{2} M^2 \\ \frac{T_{t,e}}{T_e} &= 1 + \frac{\gamma - 1}{2} M_e{}^2 \end{aligned}\right\} \tag{5}$$

Inserting equations (5) into equation (4) and assuming isoenergetic flow $\left(T_t = T_{t,e}\right)$ results in

$$\frac{u}{u_e} = \frac{M}{M_e}\sqrt{\frac{1 + \frac{\gamma - 1}{2} M_e{}^2}{1 + \frac{\gamma - 1}{2} M^2}} \tag{6}$$

which was used to calculate velocity ratios in this paper.

Integral Thicknesses

Boundary-layer momentum thickness θ and displacement thickness δ^* are defined in two-dimensional compressible flow to be

$$\theta = \int_0^\delta \frac{\rho u}{\rho_e u_e}\left(1 - \frac{u}{u_e}\right)dy \tag{7}$$

and

$$\delta^* = \int_0^\delta \left(1 - \frac{\rho u}{\rho_e u_e}\right)dy \tag{8}$$

By using the assumptions of constant static pressure and total temperature across the boundary layer, the density ratio ρ/ρ_e can be written as

$$\frac{\rho}{\rho_e} = \frac{T_e}{T} = \frac{1 + \frac{\gamma - 1}{2} M^2}{1 + \frac{\gamma - 1}{2} M_e{}^2} \tag{9}$$

Equations (6) and (9) allow the calculation of the integrands in equations (7) and (8) for each data point in the boundary layer. The integrations were performed by parabolic curve fitting through successive data points and stepwise integration of the resulting curves.

Skin-Friction Coefficient

Experimental values of the wall shearing forces were measured by the floating-element balance described earlier. Local skin friction was calculated from

$$c_f \equiv \frac{\tau_w}{q_e} = \frac{S}{Aq_e} \tag{10}$$

The balance floating element surface area A was calculated by use of the measured diameter of the floating element (9.271 mm) instead of the nominal diameter of the element plus the gap width (9.398 mm).

COMPRESSIBLE-FLOW PRESTON TUBE CALIBRATIONS

Fenter-Stalmach Equation

Fenter and Stalmach (ref. 3) derived a compressible law of the wall in the form

$$\frac{u_e}{M_e}\sqrt{5 + M_e^2}\sqrt{\frac{\rho_w}{\tau_w}}\sin^{-1}\left(\frac{M_e}{\sqrt{5 + M_e^2}}\frac{u}{u_e}\right) = 5.75 \log_{10}\left(\frac{y}{\nu_w}\sqrt{\frac{\tau_w}{\rho_w}}\right) + 5.1 \tag{11}$$

They then assumed that this law could be used as a compressible Preston tube calibration if y in equation (11) were replaced by D/2. This substitution resulted in

$$\frac{\rho_w}{\rho_e}\frac{\mu_e}{\mu_w}\frac{R_D}{M_e}\sqrt{5 + M_e^2}\sin^{-1}\left(\frac{M_e}{\sqrt{5 + M_e^2}}\frac{u}{u_e}\right) = \sqrt{\frac{\rho_w}{\rho_e}\frac{\mu_e}{\mu_w}R_D\sqrt{c_f}}\left[4.07 \log_{10}\left(\sqrt{\frac{\rho_w}{\rho_e}\frac{\mu_e}{\mu_w}R_D\sqrt{c_f}}\right) + 1.77\right. \tag{12}$$

Sigalla Equation

Sigalla (ref. 4) applied the reference-temperature hypothesis to the incompressible Preston tube calibration in the form

$$\frac{\rho D^2 \tau_w}{\mu^2} = 0.0529\left[\frac{\rho D^2}{\mu^2}\left(p_{t,m} - p\right)\right]^{0.873} \tag{13}$$

The reference temperature hypothesis states that the incompressible flow calibration (eq. (13)) can be used in compressible flow if the fluid properties are evaluated at the reference temperature T'. (See eq. (31).) Sigalla also assumed that $p_{t,m} - p$ in the compressible case would become $\frac{1}{2}\rho' u^2$. Hence, equation (13) can be written as

$$\frac{\rho'}{\rho_e}\frac{\mu_e}{\mu'} R_D \frac{u}{u_e} = 5.13\left(\sqrt{\frac{\rho'}{\rho_e}}\frac{\mu_e}{\mu'} R_D \sqrt{c_f}\right)^{1.146} \tag{14}$$

Hopkins-Keener Equation

Hopkins and Keener (ref. 1) also used the reference temperature hypothesis, but replaced $p_{t,m} - p$ in the incompressible flow expression by $\frac{\gamma}{2} p_e M^2$. Their resulting calibration can be expressed as

$$\sqrt{\frac{\rho'}{\rho_e}}\frac{\mu_e}{\mu'} R_D \frac{M}{M_e} = 5.74\left(\sqrt{\frac{\rho'}{\rho_e}}\frac{\mu_e}{\mu'} R_D \sqrt{c_f}\right)^{1.132} \tag{15}$$

Patel T' Equation

Patel's incompressible-flow calibration as given in equation (2) of reference 5 is, in the notation of this paper,

$$\log_{10}\left[\frac{\left(p_{t,m} - p\right)D^2}{4\rho\nu^2}\right] = \log_{10}\frac{\tau_w D^2}{4\rho\nu^2} + 2\log_{10}\left(1.95\log_{10}\frac{\tau_w D^2}{4\rho\nu^2} + 4.10\right) \tag{16}$$

or

$$\frac{\left(p_{t,m} - p\right)D^2}{4\rho\nu^2} = \frac{\tau_w D^2}{4\rho\nu^2}\left(1.95\log_{10}\frac{\tau_w D^2}{4\rho\nu^2} + 4.10\right)^2 \tag{17}$$

In reference 5 Patel states that his incompressible flow calibration is an improvement over Preston's original calibration (ref. 2). It should be possible to apply the reference temperature hypothesis to this improved incompressible flow law to obtain an

improved compressible flow law. By applying the reference temperature hypothesis, it is assumed that equation (17) is valid in compressible flow if the fluid properties are evaluated at the reference temperature T'. Hence,

$$\frac{u^2}{8\nu'^2} = \frac{\tau_w D^2}{4\rho'\nu'^2}\left(1.95 \log_{10} \frac{\tau_w D^2}{4\rho'\nu'^2} + 4.10\right)^2 \tag{18}$$

Note that $p_{t,m} - p$ has been replaced by $\frac{1}{2}\rho' u^2$. Finally, this equation can be written as

$$\frac{\rho'}{\rho_e}\frac{\mu_e}{\mu'} R_D \frac{u}{u_e} = \sqrt{\frac{\rho'}{\rho_e}\frac{\mu_e}{\mu'}} R_D\sqrt{c_f}\left[3.91 \log_{10}\left(\sqrt{\frac{\rho'}{\rho_e}\frac{\mu_e}{\mu'}} R_D\sqrt{c_f}\right) + 2.34\right] \tag{19}$$

Analysis of Calibrations

The compressible-flow calibration equations presented in the previous sections are composed of the following five parameters:

$$\left.\begin{aligned}
F_1 &= \frac{\rho'}{\rho_e}\frac{\mu_e}{\mu'} R_D \frac{u}{u_e} \\
F_2 &= \sqrt{\frac{\rho'}{\rho_e}\frac{\mu_e}{\mu'}} R_D\sqrt{c_f} \\
F_3 &= \frac{\rho_w}{\rho_e}\frac{\mu_e}{\mu_w}\frac{\sqrt{5 + M_e^2}}{M_e} R_D \sin^{-1}\left(\frac{M_e}{\sqrt{5 + M_e^2}}\frac{u}{u_e}\right) \\
F_4 &= \sqrt{\frac{\rho_w}{\rho_e}}\frac{\mu_e}{\mu_w} R_D\sqrt{c_f} \\
F_5 &= \sqrt{\frac{\rho'}{\rho_e'}}\frac{\mu_e}{\mu'} R_D \frac{M}{M_e}
\end{aligned}\right\} \tag{20}$$

In terms of these five parameters, the calibration equations become

$$F_3 = F_4\left(4.06 \log_{10} F_4 + 1.77\right) \qquad \text{(Fenter-Stalmach)} \qquad (21)$$

$$F_1 = 5.13F_2^{\,1.146} \qquad \text{(Sigalla)} \qquad (22)$$

$$F_5 = 5.74F_2^{\,1.132} \qquad \text{(Hopkins-Keener)} \qquad (23)$$

$$F_1 = F_2\left(3.91 \log_{10} F_2 + 2.34\right) \qquad \text{(Patel T')} \qquad (24)$$

The Sigalla and Hopkins-Keener equations can be seen to be of the same power-law form as Preston's original incompressible-flow calibration. The other two, however, are of the log-law form, which is advocated by Patel (ref. 5) as an improvement over Preston's calibration.

It is difficult to compare equations (21) to (24) directly because of the different compressibility factors. In their incompressible forms, however, equations (21) to (24) reduce to the same parameters and can be compared directly. Therefore, as M_e approaches zero, equations (21) to (24) reduce to

$$\frac{u}{u_\tau} = 5.74 \log_{10} \frac{u_\tau D}{\nu} + 3.37 \qquad \text{(Fenter-Stalmach, incompressible)} \qquad (25)$$

$$\frac{u}{u_\tau} = 7.63\left(\frac{u_\tau D}{\nu}\right)^{0.146} \qquad \text{(Sigalla, incompressible)} \qquad (26)$$

$$\frac{u}{u_\tau} = 9.30\left(\frac{u_\tau D}{\nu}\right)^{0.132} \qquad \text{(Hopkins-Keener, incompressible)} \qquad (27)$$

$$\frac{u}{u_\tau} = 5.52 \log_{10} \frac{u_\tau D}{\nu} + 4.14 \qquad \text{(Patel, incompressible)} \qquad (28)$$

and are shown in figure 2. These four calibrations are seen to be in generally good agreement for values of $u_\tau D/\nu$ between about 200 and 600 but the power laws (Sigalla

and Hopkins-Keener) and log laws (Fenter-Stalmach and Patel) diverge above this range. Preston's original data were obtained at values of $u_\tau D/\nu$ below about 320 and his power law adequately represented his data. When Patel obtained data for values of $u_\tau D/\nu$ up to about 800, he noted the deviation from Preston's power law and proposed his log law as a more accurate representation of incompressible Preston tube data over an extended range of the calibration parameters.

The power law, then, can be considered as an approximation to the log law, an approximation which is valid over a limited range of the calibration parameters. It seems reasonable, therefore, that compressible flow calibrations in the power-law form, such as those of Sigalla and Hopkins-Keener, would be less accurate over an extended calibration parameter range than the log-law forms, such as those of Fenter-Stalmach and the T' extension of Patel.

PRESENTATION OF DATA

In order to pursue the objectives of this study, three types of experimental boundary layer measurements were performed: pitot-pressure surveys, skin-friction balance measurements, and Preston tube measurements. The nominal free-stream test conditions of this study produced the local free-stream test conditions at the test stations listed in table I. Boundary-layer measurements were made at each of these 12 test conditions and are presented in the following sections.

Pitot-Pressure Surveys

The pitot-pressure data are presented in figure 3 in terms of velocity profiles in log-log form, and are listed in tables II to IV. These profiles were integrated to give the experimental displacement and momentum thicknesses (δ^* and θ, respectively), which are listed in table V.

Table V also contains estimates of the boundary-layer thickness δ of each of the profiles. The author recognizes that the term "boundary-layer thickness" is a rather nebulous quantity because of the asymptotic nature in which the velocity profile approaches the free stream. The appendix of reference 11 contains a discussion of several ways to estimate boundary-layer thickness. For the purposes of this paper, boundary-layer thickness is defined as the value of y at which the velocity u reaches 0.9999 of its local free-stream value. If another definition of δ had been assumed, the values of δ could have been as much as 20 percent different from those listed in table V. It should be noted, however, that the measured boundary-layer thickness is not used anywhere else in this paper; hence, the specific values have no effect on the results of this paper. They are presented, however, for completeness.

Experimental values of the power-law velocity profile exponent N, which is defined by $\frac{u}{u_e} \propto y^{1/N}$, were estimated from the best straight-line fit to the profiles of figure 3 and are listed in table V. A survey of available data on this subject (ref. 12) revealed that this method of estimating N was accurate to within about ±10 percent.

The variations of all the gross parameters just presented with unit Reynolds number for $M_\infty = 2.3$ and $M_\infty = 4.6$ are presented in figure 4, which reveals that all the trends look reasonable and that the data scatter is less than 2 percent.

Skin-Friction Balance Measurements

The measured local skin-friction coefficients are included in table V and are presented in figure 5 in the form of transformed skin friction c_f' as a function of transformed Reynolds number based on momentum thickness R_θ' where

$$c_f' = c_f \frac{T'}{T_e} \tag{29}$$

and

$$R_\theta' = R_\theta \frac{\mu_e}{\mu'} \tag{30}$$

The reference temperature T' used in equations (29) and (30) is the Sommer and Short (ref. 13) expression

$$\frac{T'}{T_e} = 1 + 0.035M_e^2 + 0.45\left(\frac{T_w}{T_e} - 1\right) \tag{31}$$

which for the adiabatic-wall conditions of this study, reduces to

$$\frac{T'}{T_e} = 1 + 0.1142M_e^2 \tag{32}$$

Using equation (32) and the Sutherland viscosity expression

$$\frac{\mu'}{\mu_e} = \left(\frac{T'}{T_e}\right)^{1.5} \frac{T_e + 199}{T' + 199} \tag{33}$$

allowed the data to be expressed in the transformed, or incompressible, form by equations (29) and (30), and to be compared directly with the Karman-Schoenherr incompressible skin-friction law

$$\frac{0.242}{\sqrt{C_f}} = \log_{10}\left(2R_\theta\right) \tag{34a}$$

where

$$c_f = \frac{C_f}{1 + 3.59\sqrt{C_f}} \tag{34b}$$

Stated simply, figure 5 shows the measured data transformed to the incompressible plane by the reference temperature method instead of the incompressible flow theory transformed to the compressible plane, which is the normal application of the reference-temperature hypothesis. Presenting the results in this manner allows the data for all three Mach numbers to be presented and compared with a single theory curve. Figure 5 shows that the data from all three Mach numbers collapse onto a narrow band, but this band is about 10 to 19 percent higher than the theory curve. Since the Sommer and Short method is just a T' extension of the Karman-Schoenherr law, the data, if plotted in the compressible plane, would be about the same percentage above the Sommer and Short T' theory.

Preston Tube Measurements

The primary results of this study are contained in the Preston tube measurements which are listed in tables VI to VIII. Included in this listing are the five calibrating parameters F_1, F_2, F_3, F_4, and F_5 described previously. These results are presented in graphical form and analyzed in a subsequent section.

DISCUSSION OF RESULTS

In this section the available Preston tube calibration data are compared with the four calibration equations presented earlier and with two additional equations developed in this section. Plots of the data and equations are analyzed for two characteristics: (1) the capability of the calibrating parameters to collapse the data onto a single band, and (2) the accuracy of the fit of the calibration equations through the experimental data.

Fenter-Stalmach Calibration Equation

Available supersonic, adiabatic-wall calibration data (from the present study and from refs. 1 and 3) are compared in figure 6(a) with the Fenter-Stalmach equation (eq. (21)). The data do collapse onto a single narrow band by using these parameters (F_3 and F_4), and the equation fits through the data fairly well. Note that the maximum

value of the calibration parameters of the present data is more than an order of magnitude larger than that previously obtained.

It is difficult from figure 6(a) to ascertain the accuracy with which the Fenter-Stalmach equation predicts the measured skin friction. Figure 6(b) was therefore prepared by using all the data points shown in figure 6(a). Note that there is a steady improvement in accuracy with increasing F_3, but below values of F_3 of about 10^3 there is a rapid decrease in accuracy, probably because of the inability of the small probes to measure accurately the low pitot pressures. $F_3 = 10^3$ corresponds to $F_2 \approx 10^2$, which is the point below which Hopkins and Keener (ref. 1) noticed large deviations in their data and recommended not using the Preston tube technique. Ignoring, therefore, the data below $F_3 = 10^3$, the c_f error band is generally confined to 17 to -8 percent.

Sigalla Calibration Equation

The calibration parameters used in the Sigalla equation (eq. (22)), F_1 and F_2, collapse the data fairly well onto a single band (fig. 7(a)) with about the same amount of scatter as was present in the Fenter-Stalmach parameters, F_3 and F_4, presented earlier. The Sigalla equation, however, does not represent the trend of the data at the higher values of the calibration parameters. Figure 7(b) shows that above $F_2 = 10^2$ $\left(\text{or } F_1 \approx 10^3\right)$, the percent c_f error range using the Sigalla equation is about 25 to -23.

Hopkins-Keener Calibration Equation

Figure 8(a) shows the data compared with the Hopkins-Keener equation (eq. (23)). The data here fall into two diverging bands. The limited amount of data that comprises the upper band is the high Mach number, large-tube-diameter data of the present study. Of the calibration parameters tested herein, only those of Hopkins and Keener, F_5 and F_2, resulted in such large deviations from a single band. In terms of percent c_f error, figure 8(b) shows an error range of about 50 to -15 percent for all the data above $F_2 = 10^2$ $\left(\text{or } F_5 \approx 10^3\right)$.

It should be noted that this disagreement of the upper band of data is not directly due to the high Mach number. The previous sets of data contained results at Mach numbers up to 3.7 and showed no such disagreement. Also, the present high Mach number data at the lower tube sizes $\left(\text{lower values of } F_2\right)$ tend to agree with most of the data. Similarly, this disagreement is not a tube-size effect since the lower Mach number data of the present study showed valid results even at the largest tubes tested. It is the combination, therefore, of high Mach number and large tube diameter which causes the Hopkins-Keener calibration parameters to fail to collapse the data to a single band.

Patel T' Calibration Equation

The calibration parameters for the Patel T' equation (eq. (24)) are the same as those of Sigalla, so that the data collapse is the same. Figure 9(a) shows that the Patel T' equation fits the data fairly well. The c_f percent error band for data above $F_1 = 10^3$ is seen from figure 9(b) to be about 23 to -8.

Comparison of Calibration Results

The obvious conclusion from the calibration results just presented is that the log laws of Fenter and Stalmach or Patel T' do a better job of representing the data over an extended range of the calibration parameters than do the power laws of Hopkins and Keener or Sigalla. This compressible-flow result supports the conclusion of Patel (ref. 5) for incompressible data.

One disadvantage of the log laws, however, is that c_f is not directly solvable from the equations. The experimenter must therefore use graphical or iterative means to obtain c_f from his Preston tube data. In order to obtain a calibration in which c_f can be explicitly solved for, and to obtain the best possible fit to the available data, a least-squares curve-fitting technique was applied to the data and this technique is discussed in the next section.

New Calibration Equation

Both the Fenter-Stalmach parameters, F_3 and F_4, and the Sigalla or Patel T' parameters, F_1 and F_2, gave good data collapse. (See fig. 6(a), 7(a), or 9(a).) Reference 14 reports, however, that the Fenter-Stalmach equation, used as a law of the wall, gave inaccurate results under hypersonic cold-wall conditions even though it gave reasonable results under supersonic adiabatic-wall conditions. The parameters F_1 and F_2 were therefore chosen for the least-squares curve fit so as not to exclude a priori the resulting calibration equation from use under hypersonic cold-wall conditions. Only the data whose F_2 values were greater than 10^2 were used in the curve fit.

A linear least-squares curve was tried first, and the results are shown in figure 10(a). The equation of this linear fit to the log-log plot is

$$F_2 = 0.1806 F_1^{0.9032} \tag{35}$$

This curve misses the trend of the data somewhat at the higher values of F_2; hence, the overall fit can be described as only fair. This result is a further indication that a power law is not the best representation of Preston tube data over an extended range of the calibrating parameters. Figure 10(b) shows the percent c_f errors associated with this curve. The errors for data above $F_1 = 10^3$ are generally confined to 11 to -17 percent.

To represent the data more accurately, a second-order least-squares curve fit was obtained and is shown in figure 11(a). The equation of this curve is

$$\log_{10} F_2 = 0.01659 \log_{10}^2 F_1 + 0.7665 \log_{10} F_1 - 0.4681 \tag{36}$$

The second-order term in this equation provides a slight curvature which enables the curve to follow the trend of the data very well.

The percent c_f error plot for this equation (fig. 11(b)) confirms the good overall fit to the data and shows that above $F_1 = 10^3$, the errors are generally confined to about 15 to -12 percent. Note that this percent data scatter occurs at the lower values of the calibration parameters and that the scatter is continually reduced with increasing F_1.

A third-order curve was obtained and compared with the data but gave no noticeable improvement in accuracy.

Summary of Calibration Characteristics

To get a more precise evaluation of the accuracy of each of the calibration curves discussed earlier, root-mean-square (rms) errors were obtained for each equation. The rms error used herein is

$$\text{Root-mean-square error} = \sqrt{\frac{\sum_{i=1}^{B}\left[100.0\left(\frac{c_{f,c} - c_{f,m}}{c_{f,m}}\right)\right]^2}{B}} \tag{37}$$

where B is the number of data points used in the rms calculations. Only those data points above $F_2 = 10^2$ were used in the rms calculations. These calculations along with the other general characteristics of the calibration curves discussed previously are listed in the following table for the supersonic adiabatic-wall data:

Calibration curve	Calibration parameters	Equation	Is equation directly solvable for c_f?	Data collapse	Curve fit to data	Percent error band	rms error
Fenter and Stalmach	F_3, F_4	21	No	Good	Good	17, -8	6.81
Sigalla	F_1, F_2	22	Yes	Good	Poor	25, -23	10.68
Hopkins and Keener	F_5, F_2	23	Yes	Poor	Poor	50, -15	18.32
Patel T'	F_1, F_2	24	No	Good	Good	23, -8	7.13
First-order least squares	F_1, F_2	35	Yes	Good	Fair	11, -17	6.11
Second-order least squares	F_1, F_2	36	Yes	Good	Excellent	15, -12	5.49

The rms calculations confirm the general observations made earlier that the power laws of Hopkins and Keener and Sigalla do not fit the data as well as the log laws of Fenter and Stalmach and Patel T'. As would be expected, the smallest rms errors come from the least-squares curves, the second-order curve providing the lowest rms error of those tested in this study. Because of this low rms error and the other favorable characteristics of this curve listed in the previous table, the second-order least-squares curve (eq. (36)) is presented as being the best Preston tube calibration curve for existing supersonic two-dimensional adiabatic-wall data.

Effect of Preston Tube Size

One underlying premise of Preston tube work is that the size of the tube used by the experimenter, within certain limits, does not affect his results. These limits have been investigated analytically in the past (refs. 1, 3, and 6), where estimates of the range of tube sizes which should give valid results have been published. The wide range of tube sizes used in this study allowed these theoretical tube size limits to be experimentally tested.

The theoretical maximum and minimum allowable tube sizes are given in reference 6 as

$$D_{max} = 0.375\delta \tag{38}$$

and

$$D_{min} = \frac{100\left(1.0 + 0.1142M_e^2\right)^{1.268}}{R_e\sqrt{c_f}} \tag{39}$$

Figure 12 shows the effect of tube size on the c_f calculated from the experimental F_1 values by the second-order least-squares equation (eq. (36)). Included in this figure are the theoretical tube size limits calculated from equations (38) and (39) in which nominal free-stream estimates of M_e and R_e, and theoretical estimates of δ and c_f were used. These estimates were used instead of the experimentally measured numbers because the experimenter wishing to calculate D_{max} and D_{min} in order to choose a tube size for his experiment would have no a priori knowledge of his exact conditions. Hence, using estimates was considered to be more realistic. In any event, the difference in using the measured and estimated numbers for the data in this study would result in less than 10-percent change in the calculated values of D_{max} and D_{min}. Figure 12(a) shows the $M_e = 1.975$ data. Note that there is very little variation in the Preston tube c_f except for the two smallest diameters tested. The largest tube tested was about twice as large as the theoretical maximum size but was still giving valid results.

The $M_e = 2.320$ data are shown in figure 12(b). Again, essentially constant c_f was obtained except for those tubes close to the theoretical minimum limit. The theoretical maximum diameters are larger than that of figure 12(a) because of the thicker boundary layer.

The $M_e = 4.630$ results, shown in figure 12(c), again show very little c_f variation with tube diameter for the larger tubes, but somewhat more for the smaller diameters. Note, however, that the theoretical minimum diameters are larger for this Mach number than those for the previous Mach numbers.

It would be a natural tendency when choosing a Preston tube size for use in a particular experiment to select one in the lower range of those theoretically usable. Figure 12 shows, however, that the experimenter would obtain more consistent results if he chose a larger size.

Calibration Equations Compared With the Hypersonic Cold-Wall Data

All the data used thus far (from refs. 1 and 3 and from the present study) were obtained in supersonic flow under essentially adiabatic-flow conditions. In order to test the calibration equations evaluated in this paper under hypersonic cold-wall conditions, the $M_e = 6.5$ flat-plate and $M_e \approx 7.4$ tunnel-wall data of reference 7 are presented in figure 13. The wall temperature of this test data ranged from about 32 to 51 percent of adiabatic-wall temperature.

Note that the trend of this data diverges from the calibration equations in the lower range of the calibration parameters similar to that seen in the supersonic data presented earlier. Hence, the $F_2 = 10^2$ restriction of the adiabatic-wall data appears to be applicable to this cold-wall data. Above $F_2 = 10^2$, all the calibration curves with the exception of the Fenter-Stalmach curve and possibly the Sigalla curve agree with the data fairly well. This inaccuracy of the Fenter-Stalmach law under cold-wall flow conditions supports the conclusion of reference 14, which found similar inaccuracies when using the Fenter-Stalmach law as a law of the wall.

The reason that this low-hypersonic data agree fairly well with the Hopkins-Keener calibration equation whereas the high-supersonic data of the present study do not is because of the small tube sizes used in reference 7. Comparing figures 13(c) and 8(a) reveals that for the same range of F_2 covered by the hypersonic data, the supersonic and hypersonic data are both contained within single bands.

Root-mean-square percent c_f error calculations were performed for this hypersonic data and the various calibration curves $\left(\text{above } F_2 = 10^2\right)$, and the results are presented in the following table:

Calibration curve	rms c_f error for hypersonic cold-wall data above $F_2 = 10^2$
Fenter and Stalmach	37.47
Sigalla	18.35
Hopkins and Keener	10.05
Patel T'	15.93
First-order least squares	9.22
Second-order least squares	11.45

Even though there is not enough hypersonic cold-wall data to obtain a good statistical average error, this table does indicate that the second-order least-squares curve developed in this paper gives acceptable results under at least low-hypersonic cold-wall flow conditions, as well as supersonic adiabatic-wall conditions.

CONCLUSIONS

An experimental and analytical study has been made of the accuracy of various Preston tube calibrations to determine local skin friction in two-dimensional supersonic and low-hypersonic flow. Experimental Preston tube calibration data from the present and previous studies were used to evaluate the calibration equations. The maximum value of the calibration parameters of the present data is more than an order of magnitude larger than that previously obtained; thereby, the evaluation of the various calibration equations is facilitated. The principal conclusions to be drawn from this study are

1. The Preston tube technique is highly inaccurate in the very low range of the calibration parameters. This trend was present in the four sets of data examined in this study and supports the critical minimum Preston tube diameter criterion proposed by Hopkins and Keener.

2. Above this low range, the data show a steady increase in accuracy with increasing values of the calibration parameters; hence, the use of larger Preston tubes gives more reliable results.

3. No critical maximum tube diameter was found even with tubes more than twice as large as the theoretical maximum allowable diameter.

4. Of the two forms of the calibration equation previously existing, the log laws (Fenter-Stalmach and Patel T') gave more accurate results than the power laws (Sigalla and Hopkins-Keener) over an extended range of the calibration parameters in supersonic adiabatic flow.

5. Major deficiencies in the calibration equations were found to exist for the Fenter-Stalmach equation under low-hypersonic cold-wall conditions, and for the Hopkins-Keener equation under high-supersonic large-tube-diameter conditions.

6. The second-order least-squares calibration equation developed in this paper gave the best overall results of the calibration equations evaluated and is therefore recommended for use in supersonic and low-hypersonic flow.

Langley Research Center,
National Aeronautics and Space Administration,
Hampton, Va., February 26, 1973.

REFERENCES

1. Hopkins, Edward J.; and Keener, Earl R.: Study of Surface Pitots for Measuring Turbulent Skin Friction at Supersonic Mach Numbers – Adiabatic Wall. NASA TN D-3478, 1966.

2. Preston, J. H.: The Determination of Turbulent Skin Friction by Means of Pitot Tubes. J. Roy. Aeronaut. Soc., vol. 58, no. 518, Feb. 1954, pp. 109-121.

3. Fenter, Felix W.; and Stalmach, Charles J., Jr.: The Measurement of Local Turbulent Skin Friction at Supersonic Speeds by Means of Surface Impact Pressure Probes. DRL-393, CM-878 (Contract Nord-16498), Univ. of Texas, Oct. 21, 1957.

4. Sigalla, Armand: Calibration of Preston Tubes in Supersonic Flow. AIAA J., vol. 3, no. 8, Aug. 1965, p. 1531.

5. Patel, V. C.: Calibration of the Preston Tube and Limitations on Its Use in Pressure Gradients. J. Fluid Mech., vol. 23, pt. 1, 1965, pp. 185-208.

6. Allen, Jerry M.: Critical Preston-Tube Sizes. J. Aircraft, vol. 7, no. 3, May-June 1970, pp. 285-287.

7. Keener, Earl R.; and Hopkins, Edward J.: Use of Preston Tubes for Measuring Hypersonic Turbulent Skin Friction. AIAA Paper No. 69-345, Apr. 1969.

8. Schaefer, William T., Jr.: Characteristics of Major Active Wind Tunnels at the Langley Research Center. NASA TM X-1130, 1965.

9. Allen, Jerry M.: Pitot-Probe Displacement in a Supersonic Turbulent Boundary Layer. NASA TN D-6759, 1972.

10. Paros, Jerome M.: Application of the Force-Balance Principle to Pressure and Skin Friction Sensors. 16th Annual Technical Meeting Proceedings, Inst. Environ. Sci., 1970, pp. 363-368.

11. Peterson, John B., Jr.: Boundary-Layer Velocity Profiles Downstream of Three-Dimensional Transition Trips on a Flat Plate at Mach 3 and 4. NASA TN D-5523, 1969.

12. Johnson, Charles B.; and Bushnell, Dennis M.: Power-Law Velocity-Profile-Exponent Variations With Reynolds Number, Wall Cooling, and Mach Number in a Turbulent Boundary Layer. NASA TN D-5753, 1970.

13. Sommer, Simon C.; and Short, Barbara J.: Free-Flight Measurements of Turbulent-Boundary-Layer Skin Friction in the Presence of Severe Aerodynamic Heating at Mach Numbers From 2.8 to 7.0. NACA TN 3391, 1955.

14. Allen, Jerry M.: Use of Baronti-Libby Transformation and Preston Tube Calibrations To Determine Skin Friction From Turbulent Velocity Profiles. NASA TN D-4853, 1968.

TABLE I.- TEST CONDITIONS

M_∞	$T_{t,\infty}$, °C	T_{aw}, °C	$p_{t,\infty}$, atm	R_∞ per meter	M_e	R_e per meter
2.0	41	24	0.69	8.00×10^6	1.975	7.52×10^6
2.3	66	46	.22	1.97	2.320	1.95
↓	↓	↓	.36	3.28	↓	3.24
↓	↓	↓	.72	6.56	↓	6.50
↓	↓	↓	1.09	9.84	↓	9.74
↓	↓	↓	1.45	13.12	↓	12.99
4.6	79	44	.74	1.97	4.630	1.95
↓	↓	↓	1.23	3.28	↓	3.24
↓	↓	↓	2.46	6.56	↓	6.46
↓	↓	↓	3.69	9.84	↓	9.71
↓	↓	↓	4.92	13.12	↓	12.96
↓	↓	↓	6.15	16.40	↓	16.14

TABLE II.- BOUNDARY-LAYER PROFILES FOR $M_e = 1.975$

y, cm	M	u/u_e
$R_e = 7.52 \times 10^6$ per meter		
0.018	0.610	0.398
.064	.901	.565
.119	.993	.613
.508	1.239	.732
.889	1.337	.775
1.270	1.407	.805
1.651	1.465	.828
2.032	1.522	.850
2.413	1.576	.870
2.794	1.625	.888
3.175	1.672	.905
3.556	1.741	.921
3.937	1.766	.936
4.318	1.810	.950
4.699	1.843	.961
5.080	1.885	.974
5.461	1.912	.982
5.842	1.935	.989
6.223	1.959	.995
6.604	1.967	.998
6.985	1.975	1.000
7.366	1.981	1.002
7.747	1.978	1.001
8.128	1.978	1.001
8.509	1.978	1.001
8.890	1.977	1.001
9.271	1.983	1.002
9.652	1.980	1.001
10.033	1.984	1.003

TABLE III.- BOUNDARY-LAYER PROFILES FOR $M_e = 2.320$

y, cm	M	u/u_e	M	u/u_e	M	u/u_e	M	u/u_e	M	u/u_e
	For R_e per meter of –									
	1.95×10^6		3.24×10^6		6.50×10^6		9.74×10^6		12.99×10^6	
0.018	0.955	0.545	0.998	0.566	1.042	0.587	1.078	0.603	1.093	0.610
.064	.951	.544	1.003	.568	1.043	.587	1,078	.603	1.114	.620
.119	1.073	.601	1.091	.609	1.135	.629	1.174	.646	1.204	.659
.508	1.320	.706	1.342	.715	1.397	.736	1.424	.746	1.449	.755
.889	1.427	.747	1.457	.758	1.504	.775	1.531	.785	1.554	.793
1.270	1.505	.776	1.526	.783	1.568	.797	1.598	.808	1.609	.811
1.651	1.569	.798	1.588	.804	1.627	.817	1.645	.823	1.660	.828
2.032	1.618	.814	1.636	.820	1.670	.831	1.697	.840	1.708	.843
2.413	1.657	.827	1.683	.835	1.720	.847	1.743	.854	1.759	.859
3.302	1.757	.858	1.783	.866	1.809	.874	1.836	.881	1.858	.888
4.064	1.828	.879	1.851	.886	1.892	.897	1.907	.901	1.934	.909
4.826	1.889	.896	1.919	.905	1.950	.913	1.974	.919	1.993	.924
5.588	1.965	.917	1.976	.920	2.014	.929	2.037	.935	2.054	.940
6.350	2.020	.931	2.044	.937	2.076	.945	2.090	.949	2.121	.956
7.112	2.088	.948	2.097	.950	2.129	.958	2.136	.959	2.173	.968
7.874	2.132	.958	2.147	.962	2.175	.968	2,186	.971	2.215	.977
8.636	2.187	.971	2.192	.972	2.220	.979	2.223	.979	2.243	.984
9.398	2.224	.979	2.225	.980	2.259	.987	2.257	.987	2.270	.989
10.160	2.258	.987	2.254	.986	2.278	.991	2.277	.991	2.292	.994
10.922	2.277	.991	2.292	.994	2.293	.994	2.297	.995	2.304	.997
11.684	2.292	.994	2.296	.995	2.304	.997	2.308	.998	2.307	.997
12.446	2.312	.998	2.310	.998	2.316	.999	2.313	.999	2.317	.999
13.208	2.315	.999	2.314	.999	2.318	1.000	2.316	.999	2.320	1.000
13.970	2.325	1.001	2.318	1.000	2.318	1.000	2.317	.999	2.321	1.000
14.732	2.325	1.001	2.319	1.000	2.317	.999	2.315	.999	2.321	1.000
15.240	2.325	1.001	2.318	1.000						

TABLE IV.- BOUNDARY-LAYER PROFILES FOR $M_e = 4.630$

y, cm	M	u/u_e	M	u/u_e	M	u/u_e	M	u/u_e	M	u/u_e	M	u/u_e
	For R_e per meter of –											
	1.95×10^6		3.24×10^6		6.46×10^6		9.71×10^6		12.96×10^6		16.14×10^6	
0.018	1.115	0.496	1.043	0.470	1.161	0.512	1.283	0.553	1.389	0.586	1.447	0.603
.064	1.116	.496	1.052	.473	1.211	.529	1.359	.577	1.445	.603	1.508	.621
.119	1.187	.521	1.295	.556	1.483	.614	1.555	.634	1.605	.647	1.657	.661
.508	1.839	.705	1.852	.708	1.925	.725	1.990	.738	2.048	.750	2.100	.760
.889	2.029	.746	2.037	.748	2.126	.765	2.208	.780	2.243	.786	2.298	.796
1.270	2.153	.770	2.176	.775	2.281	.793	2.365	.807	2.407	.814	2.461	.822
1.651	2.271	.791	2.311	.798	2.431	.817	2.512	.830	2.559	.836	2.614	.844
2.032	2.376	.809	2.431	.817	2.560	.836	2.637	.847	2.687	.854	2.731	.859
2.413	2.476	.824	2.546	.834	2.669	.851	2.743	.861	2.792	.867	2.842	.873
3.302	2.695	.855	2.776	.865	2.891	.878	2.976	.888	3.018	.892	3.066	.897
4.064	2.875	.877	2.961	.886	3.068	.898	3.147	.905	3.195	.910	3.235	.914
4.826	3.041	.895	3.123	.903	3.244	.914	3.304	.920	3.356	.924	3.397	.928
5.588	3.192	.910	3.261	.916	3.405	.928	3.449	.932	3.511	.937	3.565	.941
6.350	3.346	.923	3.433	.931	3.542	.939	3.616	.945	3.657	.947	3.703	.951
7.112	3.476	.934	3.580	.942	3.692	.950	3.753	.954	3.801	.957	3.849	.960
7.874	3.613	.944	3.706	.951	3.822	.959	3.882	.962	3.931	.965	3.971	.968
8.636	3.738	.953	3.834	.959	3.928	.965	4.003	.970	4.040	.972	4.087	.974
9.398	3.850	.960	3.936	.966	4.060	.973	4.134	.977	4.165	.978	4.226	.982
10.160	3.982	.968	4.079	.974	4.183	.979	4.245	.983	4.283	.984	4.337	.987
10.922	4.095	.975	4.183	.979	4.292	.985	4.332	.987	4.385	.989	4.430	.991
11.684	4.187	.980	4.296	.985	4.395	.990	4.444	.992	4.483	.994	4.522	.996
12.446	4.330	.987	4.388	.990	4.467	.993	4.514	.995	4.548	.997	4.579	.998
13.208	4.417	.991	4.461	.993	4.528	.996	4.566	.997	4.589	.998	4.616	.999
13.970	4.496	.994	4.528	.996	4.572	.998	4.595	.999	4.610	.999	4.629	1.000
14.732	4.566	.997	4.574	.998	4.597	.999	4.610	.999	4.622	1.000	4.637	1.000
15.494	4.622	1.000	4.596	.999	4.611	.999	4.619	1.000	4.626	1.000	4.640	1.000
15.621	4.623	1.000	4.600	.999	4.612	.999	4.620	1.000	4.629	1.000	4.640	1.000

TABLE V.- BOUNDARY-LAYER GROSS PARAMETERS

M_e	R_e per meter	δ^*, mm	θ, mm	δ, mm	N	R_θ per meter	c_f
1.975	7.52×10^6	14.44	4.810	70	6.85	3.62×10^4	0.001760
2.320	1.95	27.22	7.574	139	7.98	1.48	.001824
↓	3.24	26.23	7.338	138	8.40	2.38	.001760
↓	6.50	24.15	6.795	135	8.55	4.42	.001626
↓	9.74	23.24	6.576	134	9.30	6.41	.001536
↓	12.99	21.85	6.187	132	9.50	8.04	.001469
4.630	1.95	57.73	5.494	155	8.90	1.07	[a] .001029
↓	3.24	54.59	5.204	154	9.35	1.69	.000985
↓	6.46	50.09	4.808	153	10.24	3.11	.000904
↓	9.71	47.44	4.575	152	10.98	4.44	.000883
↓	12.96	45.55	4.404	151	11.50	5.71	.000861
↓	16.14	43.57	4.221	150	11.75	6.81	.000840

[a] No balance measurement was made at this Reynolds number. The c_f value listed here is an extrapolation of the measured values at the other Reynolds numbers.

TABLE VI.- PRESTON TUBE RESULTS FOR $M_e = 1.975$, $T_{t,\infty} = 41^{\circ}$ C, AND $T_w = T_{aw}$

R_e per meter	D, mm	M	u/u_e	c_f	F_1	F_2	F_3	F_4	F_5
7.52×10^6	1.27	0.891	0.559	0.001760	2.709×10^3	2.444×10^2	2.107×10^3	2.005×10^2	2.628×10^3
↓	2.38	.984	.608	↓	5.522	4.580	4.315	3.757	5.436
	10.2	1.255	.739		2.865×10^4	1.955×10^3	2.273×10^4	1.604×10^3	2.961×10^4
	17.8	1.337	.775		5.258	3.422	4.193	2.807	5.520
	25.4	1.405	.804		7.793	4.888	6.240	4.009	8.295
	33.0	1.461	.826		1.042×10^5	6.355	8.373	5.212	1.122×10^5
	40.6	1.505	.844		1.307	7.821	1.053×10^5	6.415	1.420
	48.3	1.541	.857		1.578	9.288	1.274	7.618	1.727

TABLE VII.- PRESTON TUBE RESULTS FOR $M_e = 2.320$, $T_{t,\infty} = 66^{\circ}$ C, AND $T_w = T_{aw}$

R_e per meter	D, mm	M	u/u_e	c_f	F_1	F_2	F_3	F_4	F_5
1.95×10^6	1.27	0.935	0.536	0.001824	5.468×10^2	5.541×10^1	4.024×10^2	4.362×10^1	5.226×10^2
	2.38	1.060	.595		1.138×10^3	1.038×10^2	8.432	8.175	1.111×10^3
	10.2	1.316	.704		5.753	4.433	4.325×10^3	3.490×10^2	5.886
	17.8	1.449	.755		1.080×10^4	7.757	8.182	6.107	1.134×10^4
	25.4	1.511	.778		1.588	1.108×10^3	1.208×10^4	8.725	1.690
	33.0	1.563	.796		2.112	1.441	1.612	1.134×10^3	2.272
	33.0	1.572	.799		2.120	1.441	1.619	1.134	2.285
	33.0	1.576	.800		2.124	1.441	1.623	1.134	2.291
	33.0	1.579	.801		2.126	1.441	1.625	1.134	2.295
	33.0	1.580	.802		2.127	1.441	1.626	1.134	2.297
	33.0	1.576	.800		2.124	1.441	1.623	1.134	2.291
	40.6	1.647	.824		2.691	1.773	2.065	1.396	2.947
	40.6	1.646	.823		2.689	1.773	2.064	1.396	2.944
	40.6	1.649	.824		2.692	1.773	2.067	1.396	2.950
	40.6	1.678	.834		3.234	2.105	2.487	1.658	3.565
	48.3	1.671	.831		3.225	2.105	2.479	1.658	3.550
	48.3	1.678	.834		3.233	2.105	2.486	1.658	3.564
	48.3	1.667	.830		3.220	2.105	2.474	1.658	3.541
3.24×10^6	1.27	.985	.560	.001760	9.515×10^2	9.060×10^1	7.021×10^2	7.133×10^1	9.168×10^2
	2.38	1.087	.607		1.934×10^3	1.698×10^2	1.435×10^3	1.337×10^2	1.896×10^3
	10.2	1.357	.721		9.797	7.248	7.385	5.707	1.011×10^4
	17.8	1.476	.765		1.821×10^4	1.268×10^3	1.382×10^4	9.987	1.924
	25.4	1.558	.794		2.699	1.812	2.060	1.427×10^3	2.901
	25.4	1.556	.793		2.697	1.812	2.058	1.427	2.897
	25.4	1.548	.791		2.687	1.812	2.050	1.427	2.882
	25.4	1.544	.789		2.683	1.812	2.045	1.427	2.875
	25.4	1.551	.792		2.691	1.812	2.052	1.427	2.888
	33.0	1.602	.809		3.574	2.356	2.735	1.855	2.877
	33.0	1.609	.811		3.585	2.356	2.745	1.855	3.895
	33.0	1.615	.813		3.594	2.356	2.753	1.855	3.909
	33.0	1.609	.811		3.585	2.356	2.745	1.855	3.895
	40.6	1.663	.829		4.509	2.899	3.464	2.283	4.956
	40.6	1.677	.833		4.533	2.899	3.485	2.283	4.996
	40.6	1.671	.832		4.523	2.899	3.476	2.283	4.979
	48.3	1.704	.842		5.437	3.443	4.188	2.711	6.028
	48.3	1.711	.844		5.451	3.443	4.200	2.711	6.052
	48.3	1.699	.840		5.428	3.443	4.180	2.711	6.012
	48.3	1.705	.842		5.440	3.443	4.190	2.711	6.033
6.50×10^6	1.27	1.033	.582	.001626	1.982×10^3	1.744×10^2	1.466×10^3	1.373×10^2	1.925×10^3
	2.38	1.129	.626		3.992	3.267	2.969	2.572	3.943
	10.2	1.414	.742		2.021×10^4	1.395×10^3	1.528×10^4	1.098×10^3	2.108×10^4
	17.8	1.520	.781		3.720	2.441	2.832	1.922	3.966
	25.4	1.581	.802		5.457	3.487	4.170	2.745	5.893
	25.4	1.605	.810		5.511	3.487	4.218	2.745	5.982
	25.4	1.599	.808		5.498	3.487	4.206	2.745	5.960
	33.0	1.655	.826		7.310	4.533	5.613	3.569	8.019
	33.0	1.643	.822		7.275	4.533	5.582	3.569	7.961
	33.0	1.648	.824		7.290	4.533	5.595	3.569	7.986

TABLE VII.- PRESTON TUBE RESULTS FOR $M_e = 2.320$, $T_{t,\infty} = 66^{\circ}$ C, AND $T_w = T_{aw}$ – Concluded

R_e per meter	D, mm	M	u/u_e	c_f	F_1	F_2	F_3	F_4	F_5
6.50×10^6	40.6	1.701	0.841	0.001626	9.155×10^4	5.579×10^3	7.050×10^4	4.393×10^3	1.014×10^5
	40.6	1.725	.848		9.238	5.579	7.125	4.393	1.029
	40.6	1.716	.845		9.206	5.579	7.095	4.393	1.023
	48.3	1.738	.852		1.102×10^5	6.625	8.507	5.216	1.231
	48.3	1.763	.860		1.118	6.625	8.595	5.216	1.248
	48.3	1.734	.851		1.101	6.625	8.494	5.216	1.228
	48.3	1.745	.854		1.105	6.625	8.530	5.216	1.236
9.74×10^6	1.27	1.058	.594	.001536	3.032×10^3	2.542×10^2	2.246×10^3	2.002×10^2	2.958×10^3
	2.38	1.158	.639		6.109	4.764	4.551	3.751	6.067
	10.2	1.436	.751		3.065×10^4	2.034×10^3	2.321×10^4	1.601×10^3	3.212×10^4
	17.8	1.541	.788		5.632	3.559	4.293	2.802	6.031
	25.4	1.608	.811		8.277	5.084	6.337	4.003	8.990
	25.4	1.625	.817		8.335	5.084	6.388	4.003	9.086
	25.4	1.599	.808		8.246	5.084	6.310	4.003	8.939
	25.4	1.608	.811		8.277	5.084	6.337	4.003	8.990
	25.4	1.628	.817		8.344	5.084	6.396	4.003	9.101
	25.4	1.617	.814		8.308	5.084	6.364	4.003	9.040
	33.0	1.674	.832		1.105×10^5	6.610	8.491	5.204	1.217×10^5
	33.0	1.667	.830		1.102	6.610	8.465	5.204	1.212
	33.0	1.672	.832		1.104	6.610	8.484	5.204	1.215
	33.0	1.663	.829		1.100	6.610	8.450	5.204	1.209
	33.0	1.668	.830		1.102	6.610	8.469	5.204	1.212
	40.6	1.739	.853		1.393	8.135	1.075×10^5	6.405	1.556
	40.6	1.716	.845		1.381	8.135	1.064	6.405	1.535
	40.6	1.727	.849		1.387	8.135	1.070	6.405	1.545
	48.3	1.754	.857		1.663	9.660	1.285	7.606	1.863
	48.3	1.748	.855		1.659	9.660	1.282	7.606	1.857
	48.3	1.759	.859		1.665	9.660	1.287	7.606	1.868
	48.3	1.752	.857		1.662	9.660	1.284	7.606	1.861
12.99×10^6	1.27	1.073	.601	.001469	4.089×10^3	3.315×10^2	3.032×10^2	2.610×10^2	3.999×10^3
	2.38	1.179	.648		8.262	6.212	6.162	4.891	8.236
	10.2	1.447	.755		4.108×10^4	2.652×10^3	3.113×10^4	2.088×10^3	4.315×10^4
	17.8	1.558	.794		7.565	4.641	5.774	3.654	8.131
	25.4	1.624	.816		1.111×10^5	6.630	8.515	5.220	1.211×10^5
	25.4	1.634	.819		1.115	6.630	8.551	5.220	1.218
	25.4	1.617	.814		1.108	6.630	8.485	5.220	1.205
	33.0	1.679	.834		1.476	8.619	1.135×10^5	6.786	1.627
	33.0	1.668	.831		1.470	8.619	1.130	6.786	1.617
	33.0	1.675	.833		1.473	8.619	1.133	6.786	1.623
	40.6	1.741	.853		1.858	1.061×10^4	1.425	8.352	2.058
	40.6	1.726	.849		1.848	1.061	1.425	8.352	2.058
	40.6	1.733	.851		1.853	1.061	1.430	8.352	2.067
	40.6	1.722	.847		1.845	1.061	1.423	8.352	2.054
	48.3	1.767	.861		2.227	1.260	1.722	9.918	2.503
	48.3	1.773	.863		2.232	1.260	1.727	9.918	2.512
	48.3	1.757	.858		2.219	1.260	1.715	9.918	2.489
	48.3	1.763	.860		2.224	1.260	1.719	9.918	2.497

TABLE VIII.- PRESTON TUBE RESULTS FOR $M_e = 4.630$, $T_{t,\infty} = 79^{\circ}$ C, AND $T_w = T_{aw}$

R_e, per meter	D,* mm	M	u/u_e	c_f	F_1	F_2	F_3	F_4	F_5
1.95×10^6	1.27	1.301	0.558	0.001029	1.201×10^2	1.281×10^1	7.030×10^1	8.420×10^0	1.122×10^2
	2.38	1.306	.560		2.257	2.401	1.322×10^2	1.578×10^1	2.111
	10.2	1.742	.682		1.174×10^3	1.025×10^2	7.064	6.736	1.202×10^3
	17.8	1.904	.720		2.167	1.793	1.318×10^3	1.179×10^2	2.299
	25.4	2.009	.742		3.192	2.562	1.953	1.684	3.465
	33.0	2.144	.769		4.297	3.331	2.652	2.189	4.807
	40.6	2.377	.809		5.567	4.099	3.484	2.695	6.561
	48.3	2.327	.801		6.543	4.868	4.083	3.200	7.626
	48.3	2.408	.814		6.650	4.868	4.170	3.200	7.893
3.24×10^6	1.27	.910	.419	.000985	1.499×10^2	2.086×10^1	1.352×10^1	1.371×10^1	1.307×10^2
	2.38	1.272	.549		3.683	3.908	2.152×10^2	2.569	3.422
	10.2	1.813	.699		2.002×10^3	1.669×10^2	1.210×10^3	1.097×10^2	2.082×10^3
	17.8	1.956	.731		3.663	2.920	2.234	1.919	3.930
	25.4	2.103	.761		5.446	4.171	3.352	2.742	6.037
	33.0	2.255	.789		7.338	5.423	4.559	3.564	8.415
	40.6	2.440	.819		9.377	6.674	5.891	4.387	1.121×10^4
	40.6	2.428	.817		9.355	6.674	5.873	4.387	1.115
	48.3	2.477	.824		1.121×10^4	7.925	7.059	5.210	1.351
	48.3	2.481	.825		1.122	7.925	7.065	5.210	1.353
	48.3	2.471	.823		1.120	7.925	7.048	5.210	1.348
6.46×10^6	1.27	1.129	.501	.000904	3.576×10^2	3.990×10^1	2.073×10^2	2.623×10^1	3.235×10^2
	1.27	1.138	.504		3.599	3.990	2.087	2.623	3.261
	2.38	1.434	.599		8.026	7.478	4.737	4.916	7.699
	2.38	1.396	.588		7.876	7.478	4.638	4.916	7.498
	10.2	1.913	.722		4.126×10^3	3.192×10^2	2.510×10^3	2.098×10^2	4.385×10^3
	10.2	1.879	.714		4.084	3.192	2.478	2.098	4.307
	17.8	2.107	.762		7.617	5.586	4.690	3.672	8.451
	17.8	2.085	.757		7.575	5.586	4.658	3.672	8.364
	25.4	2.269	.791		1.130×10^4	7.981	7.028	5.246	1.300×10^4
	25.4	2.302	.797		1.139	7.981	7.094	5.246	1.320
	33.0	2.394	.812		1.508	1.038×10^3	9.445	6.820	1.783
	33.0	2.450	.820		1.524	1.038	9.578	6.820	1.825
	40.6	2.558	.836		1.912	1.277	1.209×10^4	8.394	2.346
	40.6	2.572	.838		1.916	1.277	1.213	8.394	2.359
	48.3	2.638	.847		2.300	1.516	1.462	9.967	2.872
	48.3	2.607	.843		2.289	1.516	1.452	9.967	2.839
9.71×10^6	1.27	1.280	.552	.000883	5.923×10^2	5.923×10^1	3.463×10^2	3.894×10^1	5.511×10^2
	2.38	1.507	.621		1.249×10^3	1.110×10^2	7.402	7.296	1.216×10^3
	10.2	1.996	.740		6.351	4.738	3.883×10^3	3.115×10^2	6.875
	17.8	2.205	.780		1.172×10^4	8.292	7.258	5.451	1.329×10^4
	25.4	2.342	.803		1.724	1.185×10^3	1.077×10^4	7.787	2.016
	25.4	2.382	.810		1.738	1.185	1.088	7.787	2.051
	25.4	2.374	.808		1.735	1.185	1.086	7.787	2.044
	33.0	2.507	.829		2.313	1.540	1.459	1.012×10^3	2.807
	33.0	2.521	.831		2.319	1.540	1.464	1.012	2.822
	33.0	2.508	.829		2.314	1.540	1.459	1.012	2.807
	33.0	2.521	.831		2.319	1.540	1.464	1.012	2.822

TABLE VIII.- PRESTON TUBE RESULTS FOR $M_e = 4.630$, $T_{t,\infty} = 79^\circ$ C, AND $T_w = T_{aw}$ – Concluded

R_e per meter	D, mm	M	u/u_e	c_f	F_1	F_2	F_3	F_4	F_5
9.71×10^6	33.0	2.517	0.830	0.000883	2.317×10^4	1.540×10^3	1.462×10^4	1.012×10^3	2.817×10^4
	40.6	2.621	.845		2.902	1.895	1.843	1.246	3.612
	40.6	2.631	.846		2.907	1.895	1.847	1.246	3.625
	40.6	2.636	.847		2.909	1.895	1.848	1.246	3.631
	40.6	2.634	.847		2.908	1.895	1.848	1.246	3.629
	48.3	2.719	.858		3.499	2.251	2.234	1.480	4.448
	48.3	2.678	.852		3.477	2.251	2.215	1.480	4.381
	48.3	2.699	.855		3.488	2.251	2.224	1.480	4.415
	48.3	2.701	.855		3.490	2.251	2.226	1.480	4.419
12.96×10^6	1.27	1.352	.575	.000861	8.230×10^2	7.807×10^1	4.833×10^2	5.132×10^1	7.766×10^2
	2.38	1.545	.631		1.695×10^3	1.463×10^2	1.007×10^3	9.617	1.663×10^3
	10.2	2.060	.752		8.623	6.245	5.293	4.105×10^2	9.467
	17.8	2.270	.791		1.587×10^4	1.093×10^3	9.866	7.184	1.826×10^4
	25.4	2.422	.816		2.338	1.561	1.467×10^4	1.026×10^3	2.783
	25.4	2.412	.814		2.333	1.561	1.463	1.026	2.771
	25.4	2.399	.812		2.327	1.561	1.459	1.026	2.756
	25.4	2.417	.815		2.335	1.561	1.465	1.026	2.777
	33.0	2.526	.832		3.097	2.030	1.956	1.334	3.773
	33.0	2.545	.834		3.107	2.030	1.964	1.334	3.801
	40.6	2.681	.853		3.909	2.498	2.490	1.642	4.929
	40.6	2.675	.852		3.906	2.498	2.488	1.642	4.919
	40.6	2.672	.852		3.904	2.498	2.486	1.642	4.912
	40.6	2.666	.851		3.901	2.498	2.483	1.642	4.902
	48.3	2.760	.863		4.697	2.967	3.005	1.950	6.024
	48.3	2.726	.859		4.674	2.967	2.986	1.950	5.953
	48.3	2.736	.860		4.681	2.967	2.991	1.950	5.974
	48.3	2.716	.857		4.667	2.967	2.979	1.950	5.931
16.14×10^6	1.27	1.391	.587	.000840	1.046×10^3	9.600×10^1	6.159×10^2	6.310×10^1	9.951×10^2
	2.38	1.576	.640		2.139	1.799×10^2	1.274×10^3	1.183×10^2	2.113×10^3
	10.2	2.118	.764		1.090×10^4	7.680	6.714	5.048	1.212×10^4
	17.8	2.309	.798		1.992	1.344×10^3	1.242×10^4	8.835	2.313
	25.4	2.458	.821		2.931	1.920	1.843	1.262×10^3	3.517
	25.4	2.433	.818		2.917	1.920	1.832	1.262	3.481
	25.4	2.469	.823		2.937	1.920	1.848	1.262	3.533
	25.4	2.445	.819		2.924	1.920	1.837	1.262	3.498
	33.0	2.589	.840		3.898	2.496	2.470	1.641	4.816
	33.0	2.576	.839		3.890	2.496	2.463	1.641	4.792
	33.0	2.576	.839		3.890	2.496	2.463	1.641	4.792
	40.6	2.698	.855		4.881	3.072	3.113	2.019	6.177
	40.6	2.702	.856		4.885	3.072	3.116	2.019	6.188
	40.6	2.712	.857		4.892	3.072	3.122	2.019	6.209
	40.6	2.707	.856		4.888	3.072	3.118	2.019	6.197
	48.3	2.796	.867		5.879	3.648	3.770	2.398	7.601
	48.3	2.761	.863		5.851	3.648	3.744	2.398	7.507
	48.3	2.759	.863		5.849	3.648	3.743	2.398	7.503
	48.3	2.741	.861		5.834	3.648	3.729	2.398	7.453

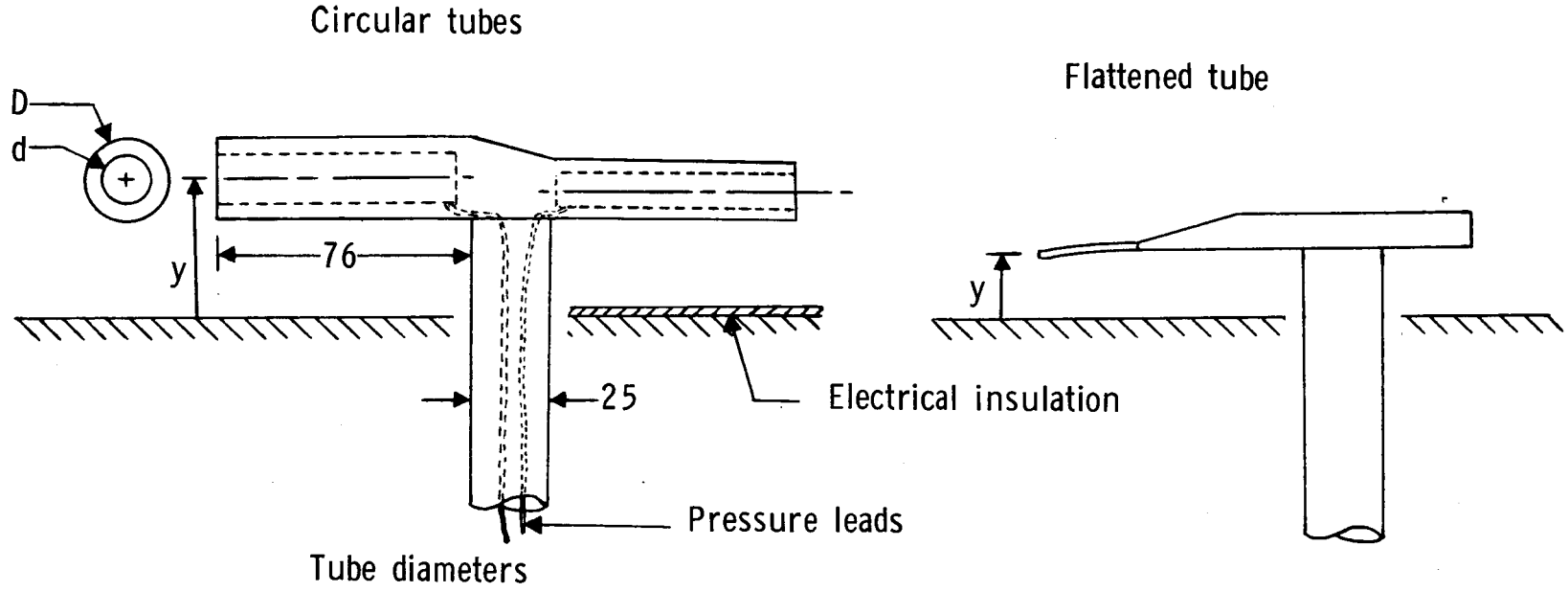

Tube	d	D	d/D
1	0.76	1.27	.60
2	1.40	2.38	.59
3	6.10	10.2	.60
4	10.7	17.8	.60
5	15.2	25.4	.60
6	19.8	33.0	.60
7	24.4	40.6	.60
8	29.0	48.3	.60

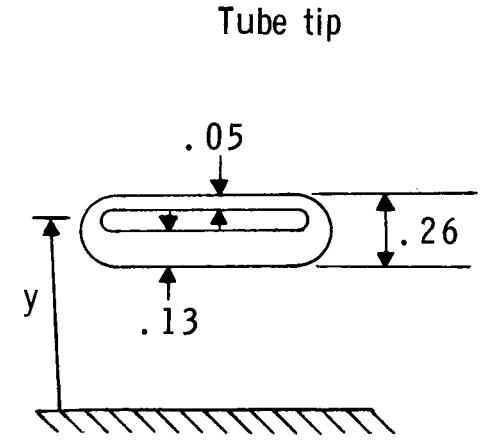

Figure 1.- Tube sketches. All dimensions are in millimeters.

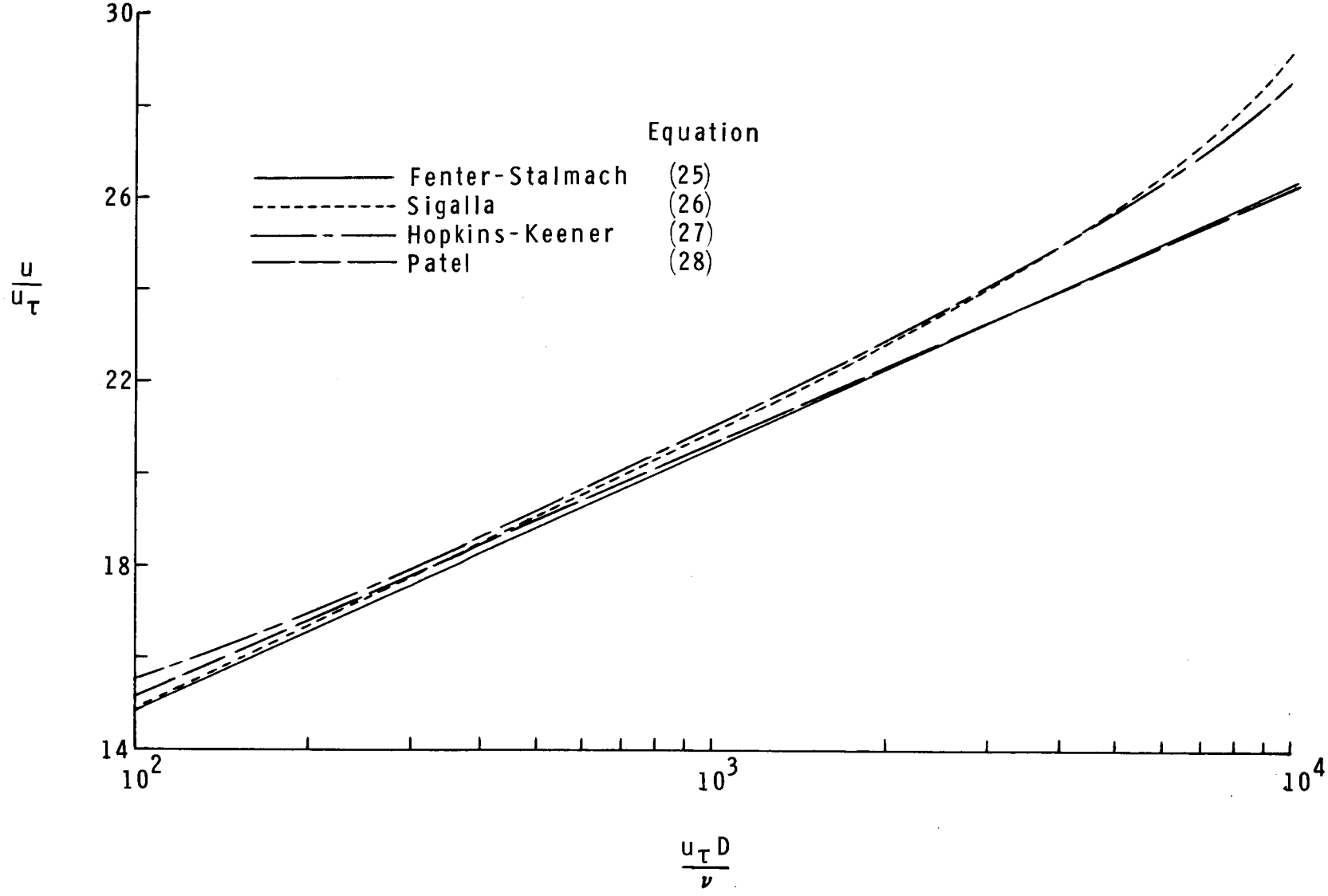

Figure 2.- Comparison of Preston tube calibrations for $M_e = 0$.

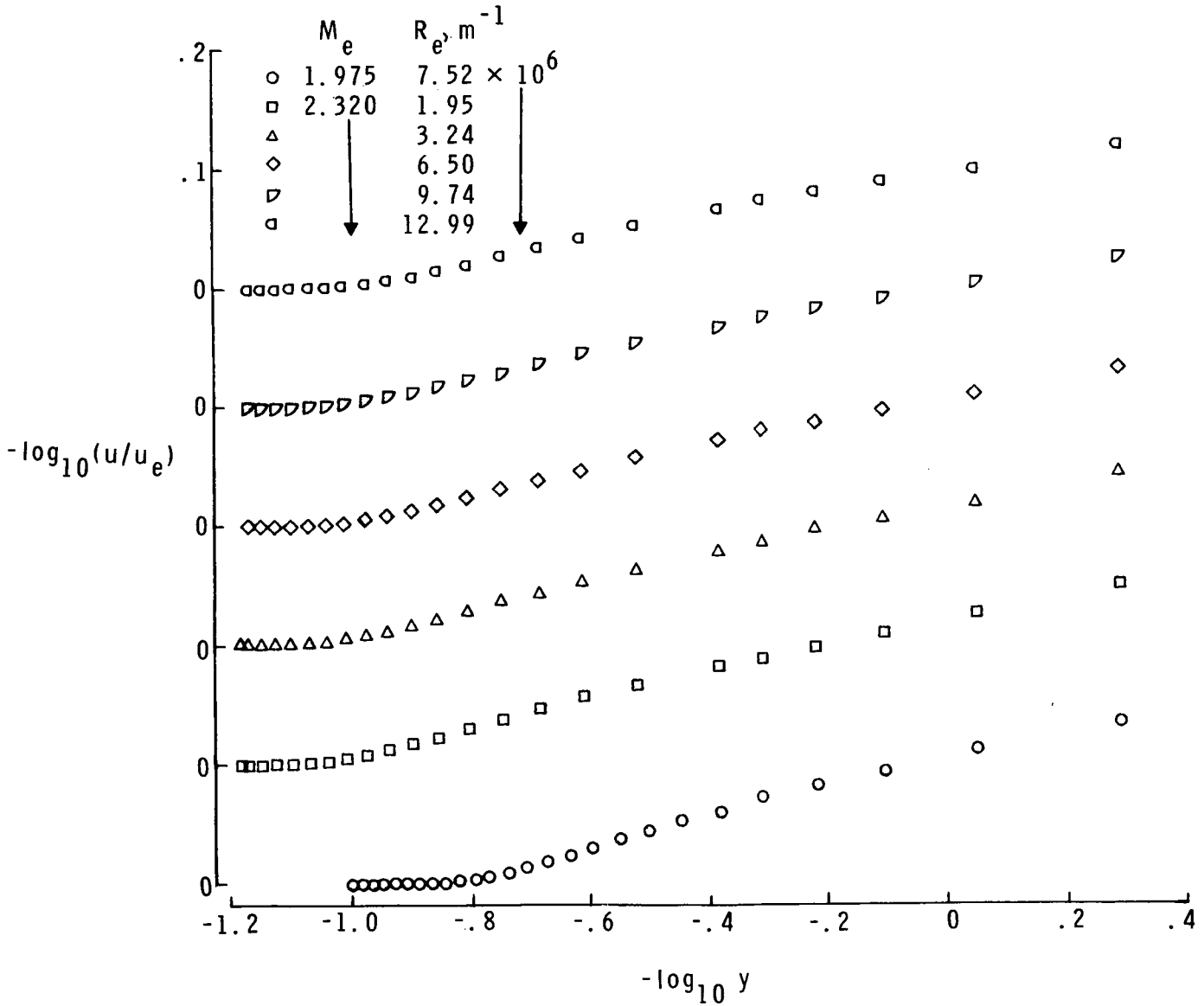

(a) M_e = 1.975 and 2.320.

Figure 3.- Velocity profiles.

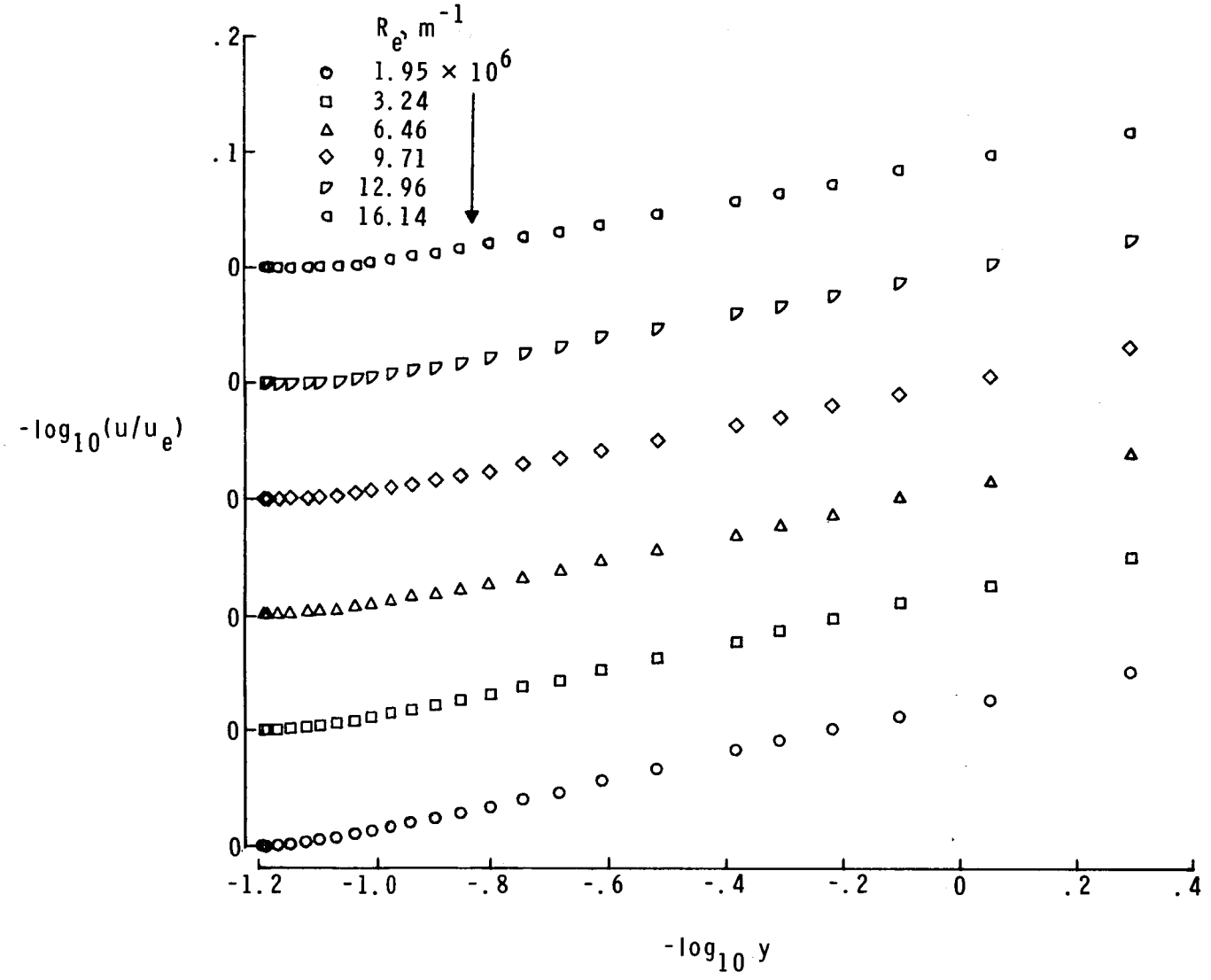

(b) $M_e = 4.630$.

Figure 3.- Concluded.

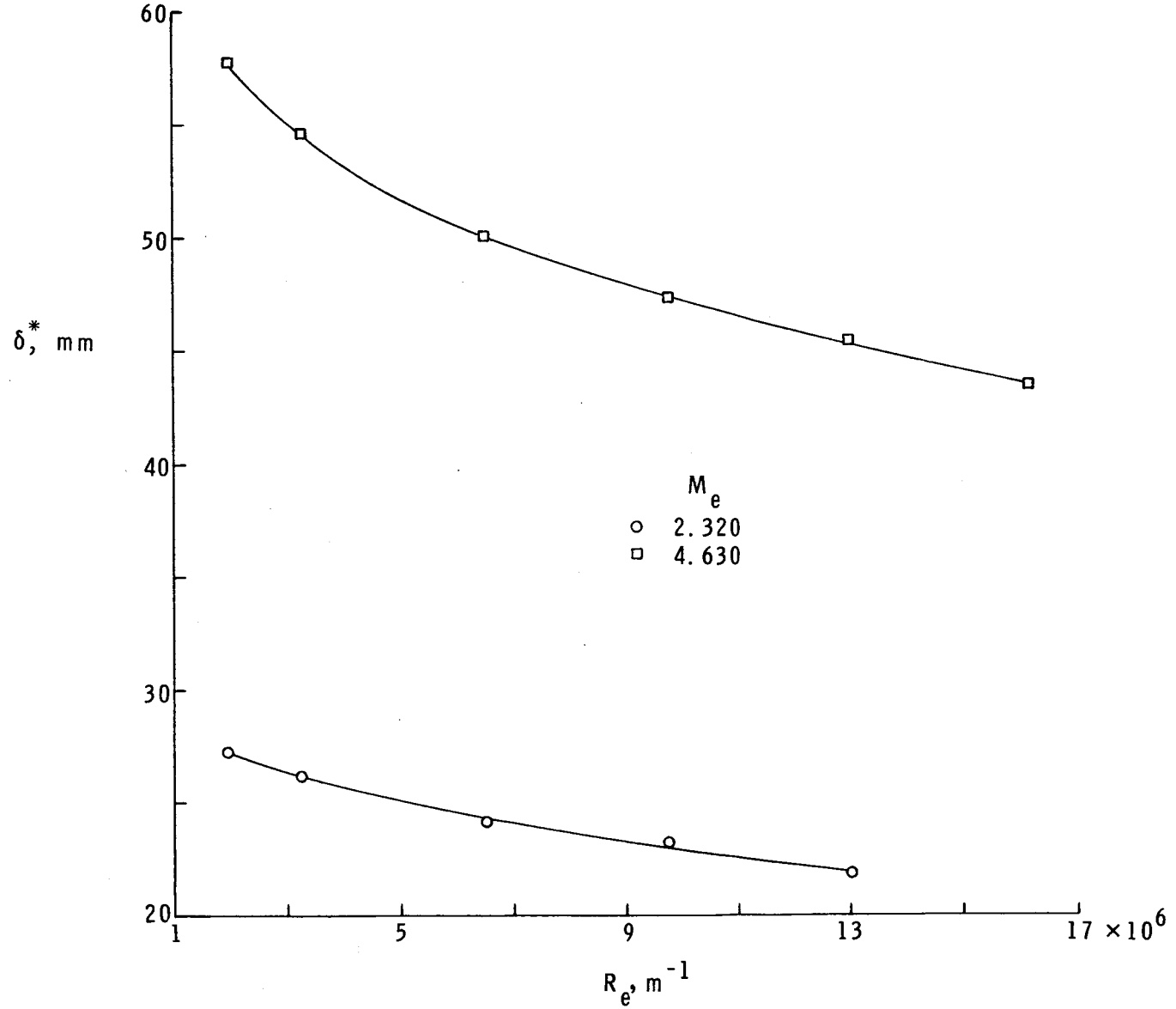

(a) Displacement thickness.

Figure 4.- Effect of unit Reynolds number on gross parameters.

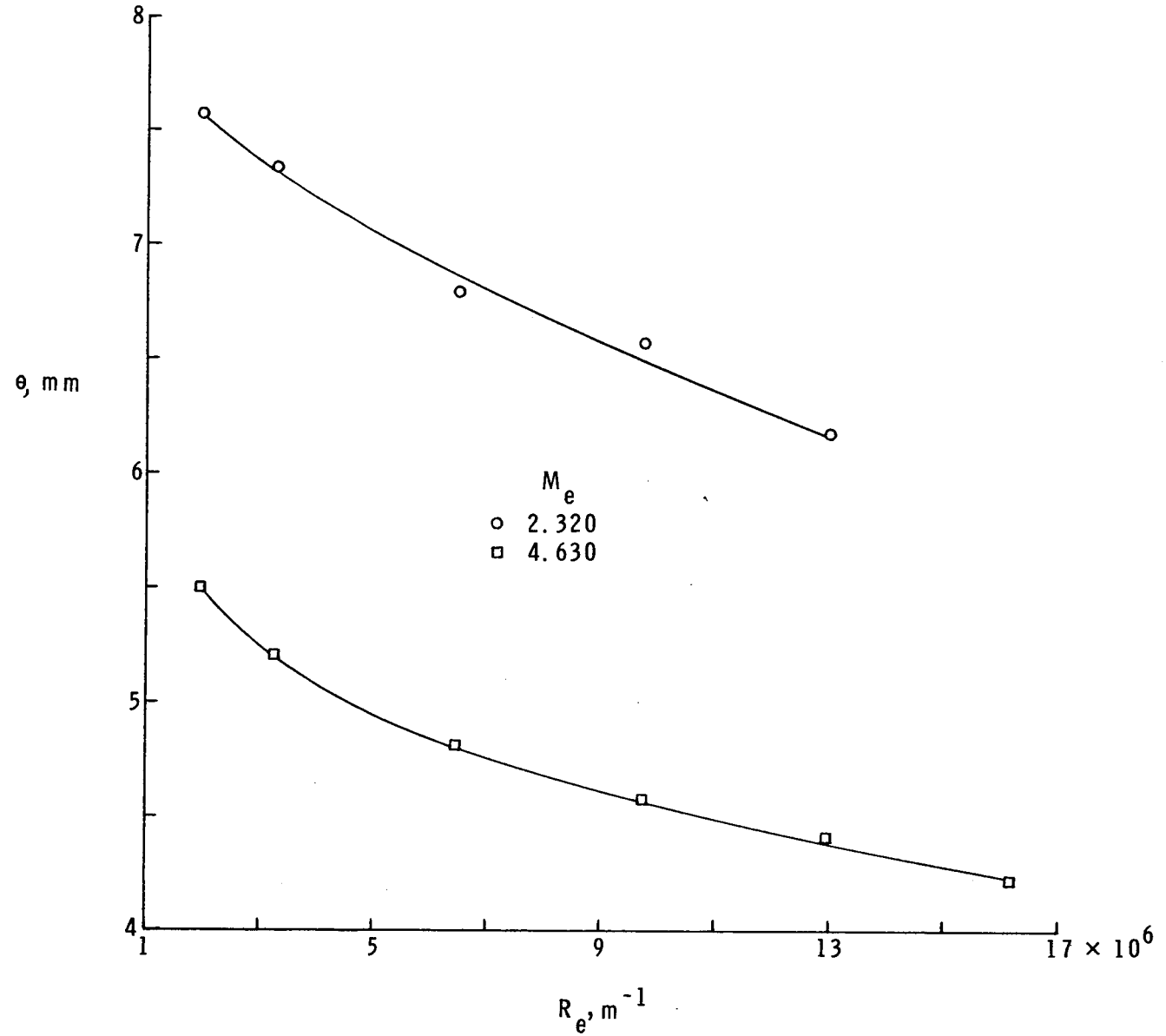

(b) Momentum thickness.

Figure 4.- Continued.

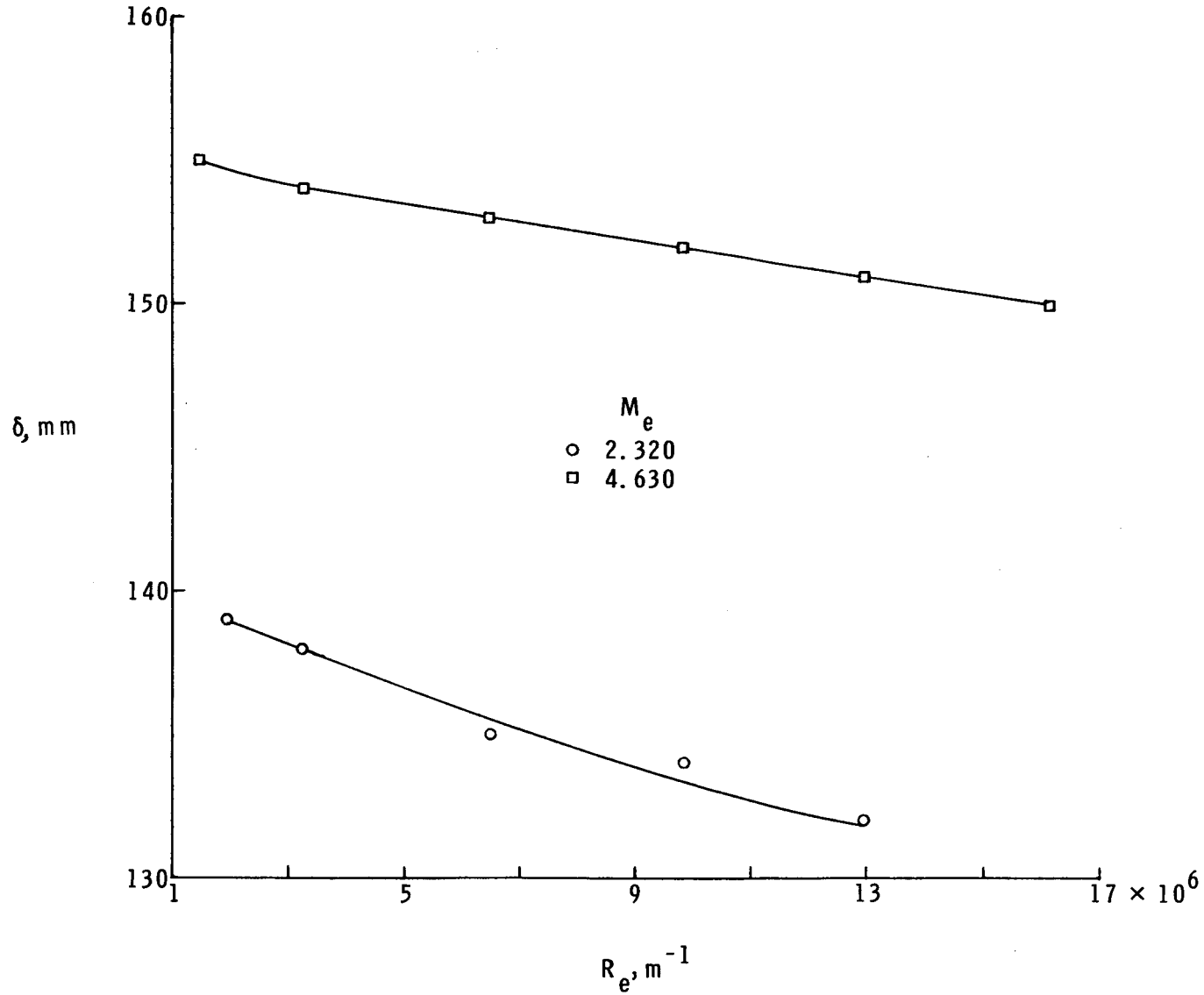

(c) Boundary-layer thickness.

Figure 4.- Continued.

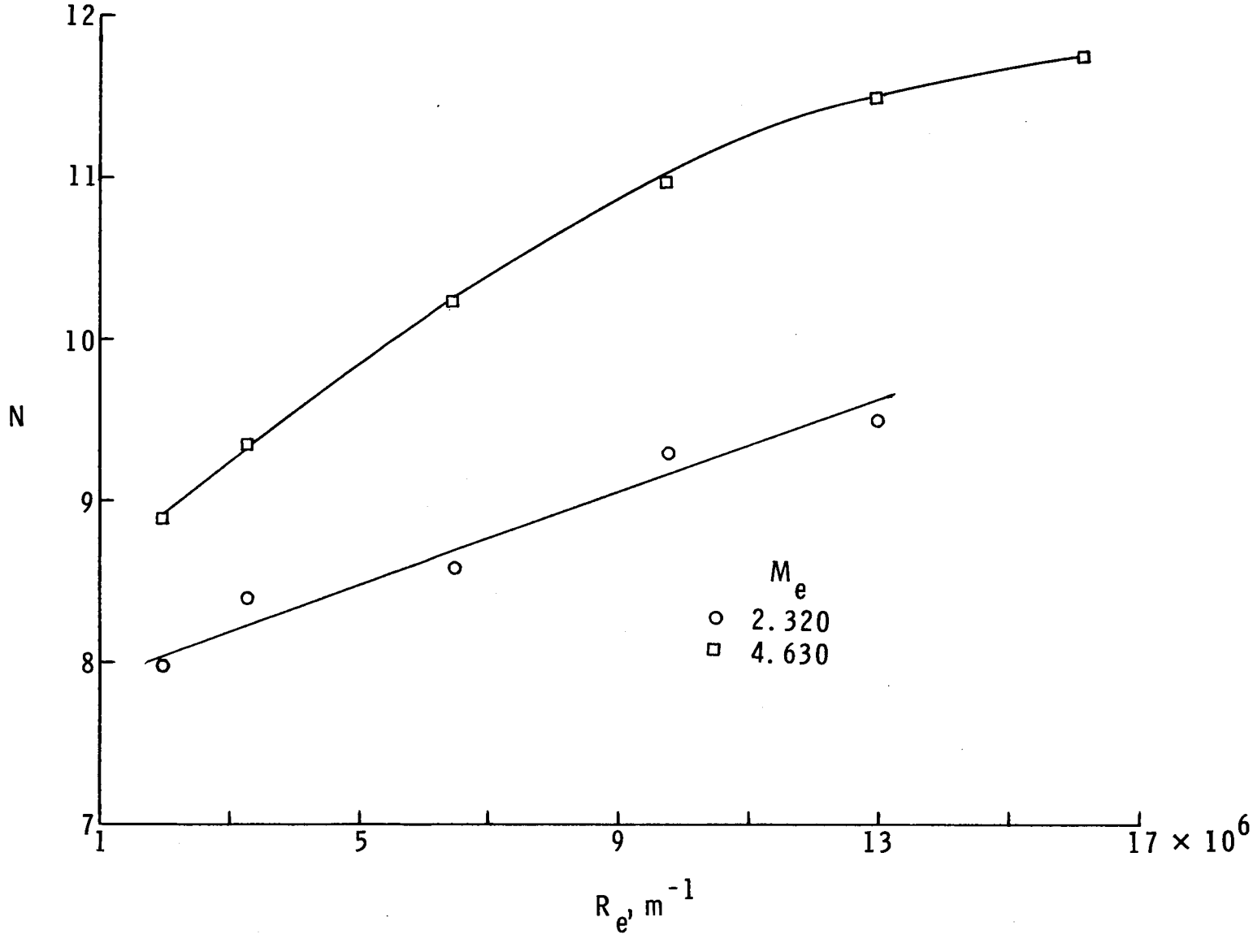

(d) Power-law velocity-profile exponent.

Figure 4.- Concluded.

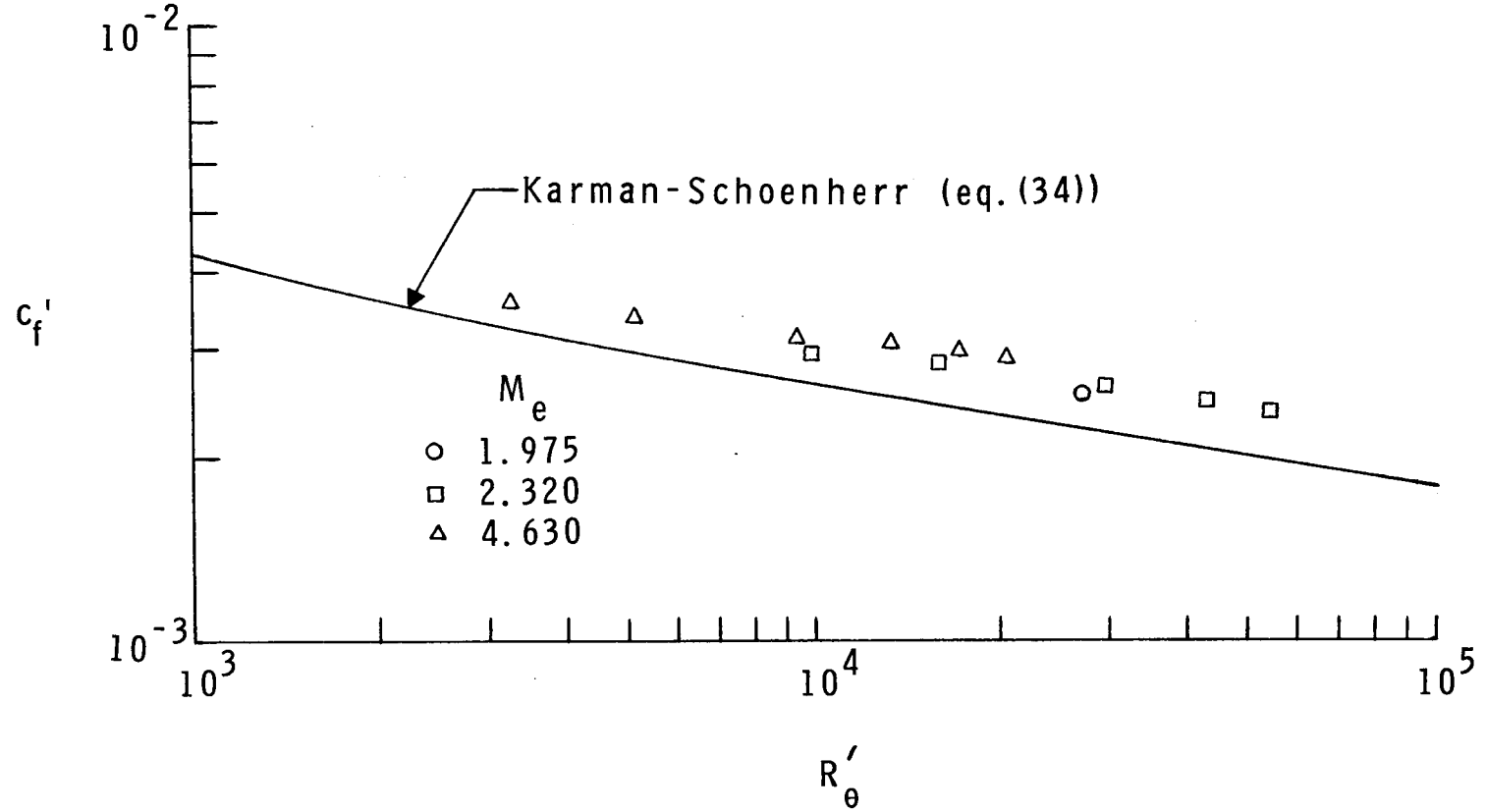

Figure 5.- Transformed local skin friction.

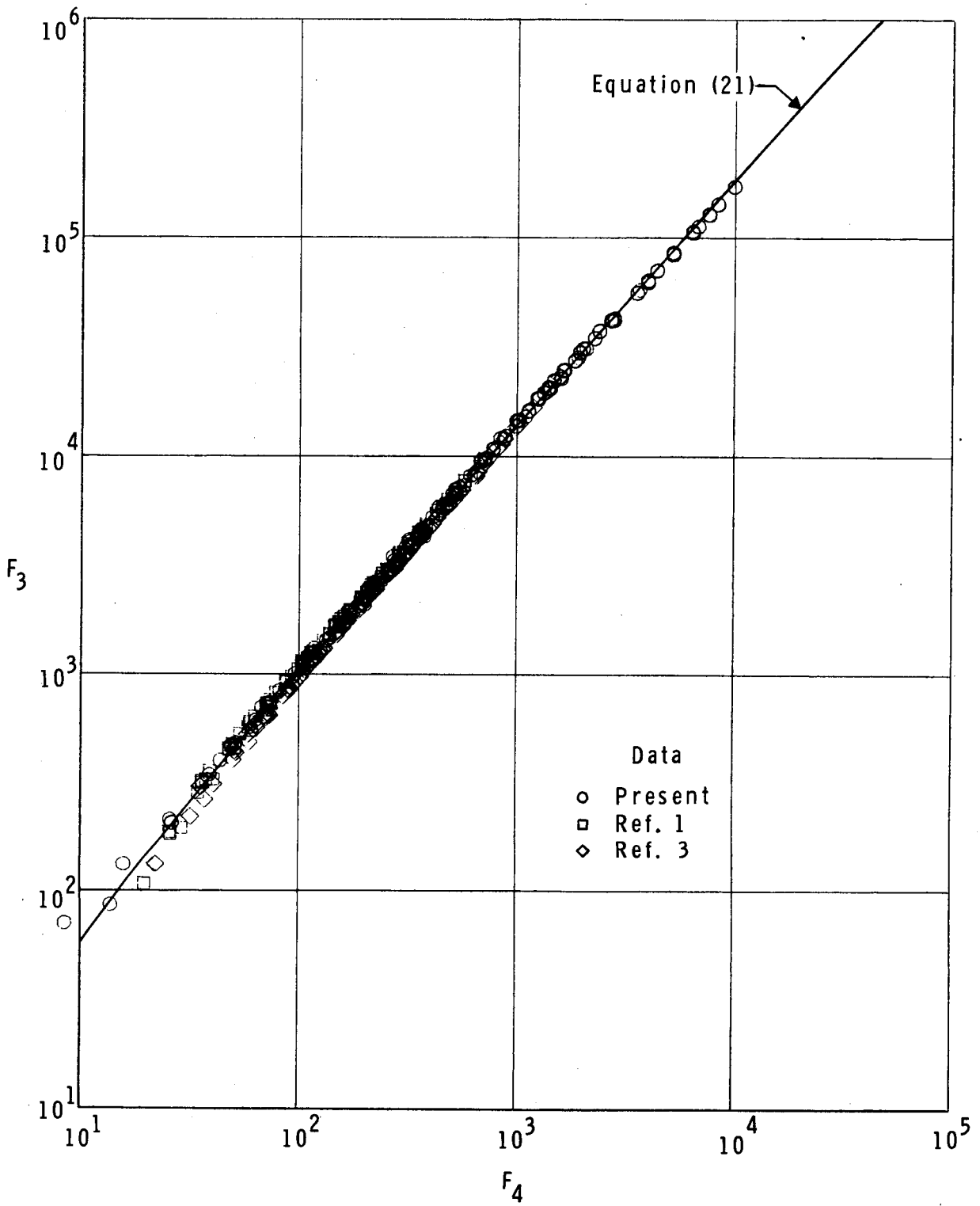

(a) Calibration parameters.

Figure 6.- Fenter-Stalmach calibration equation.

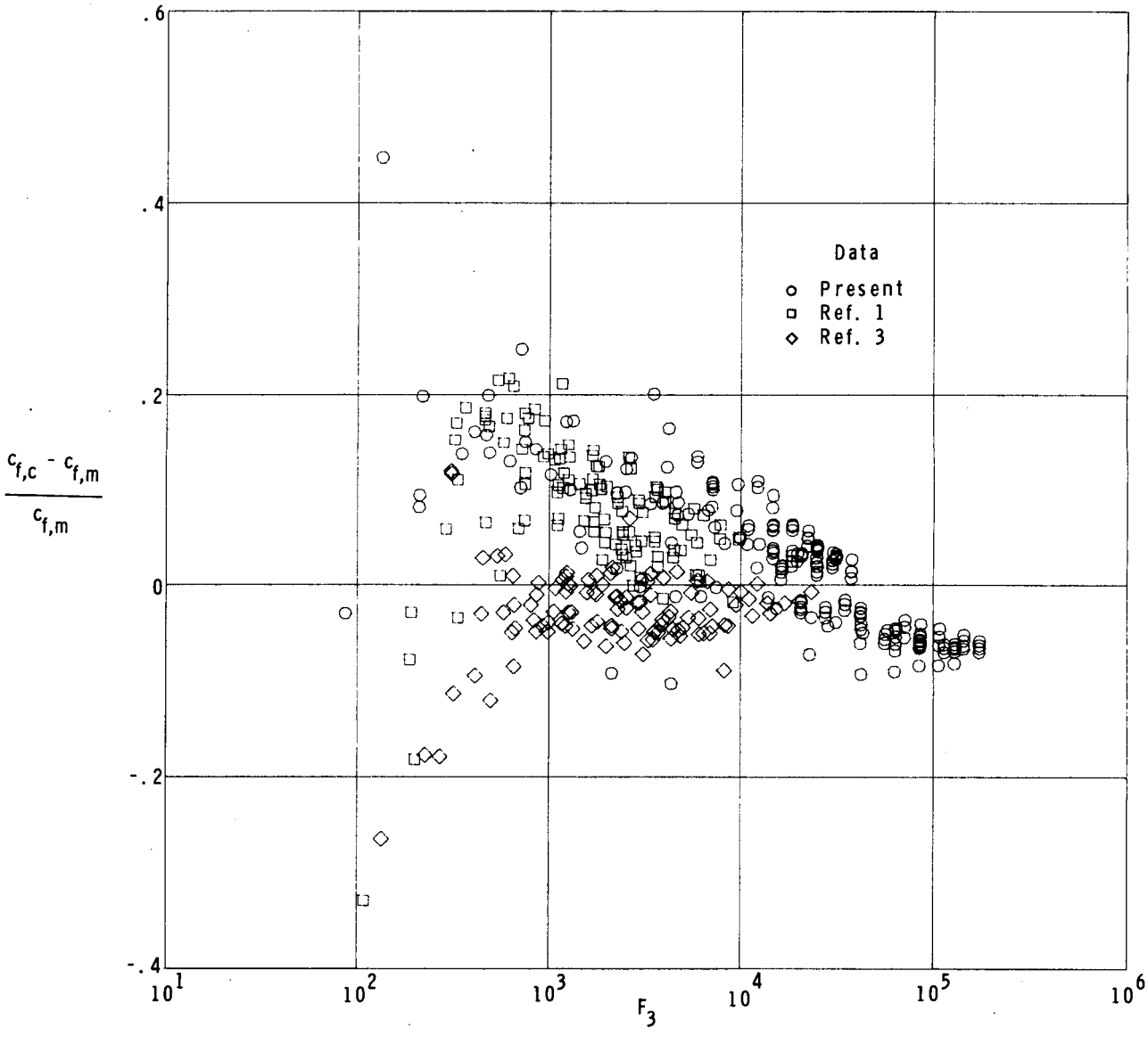

(b) c_f error.

Figure 6.- Concluded.

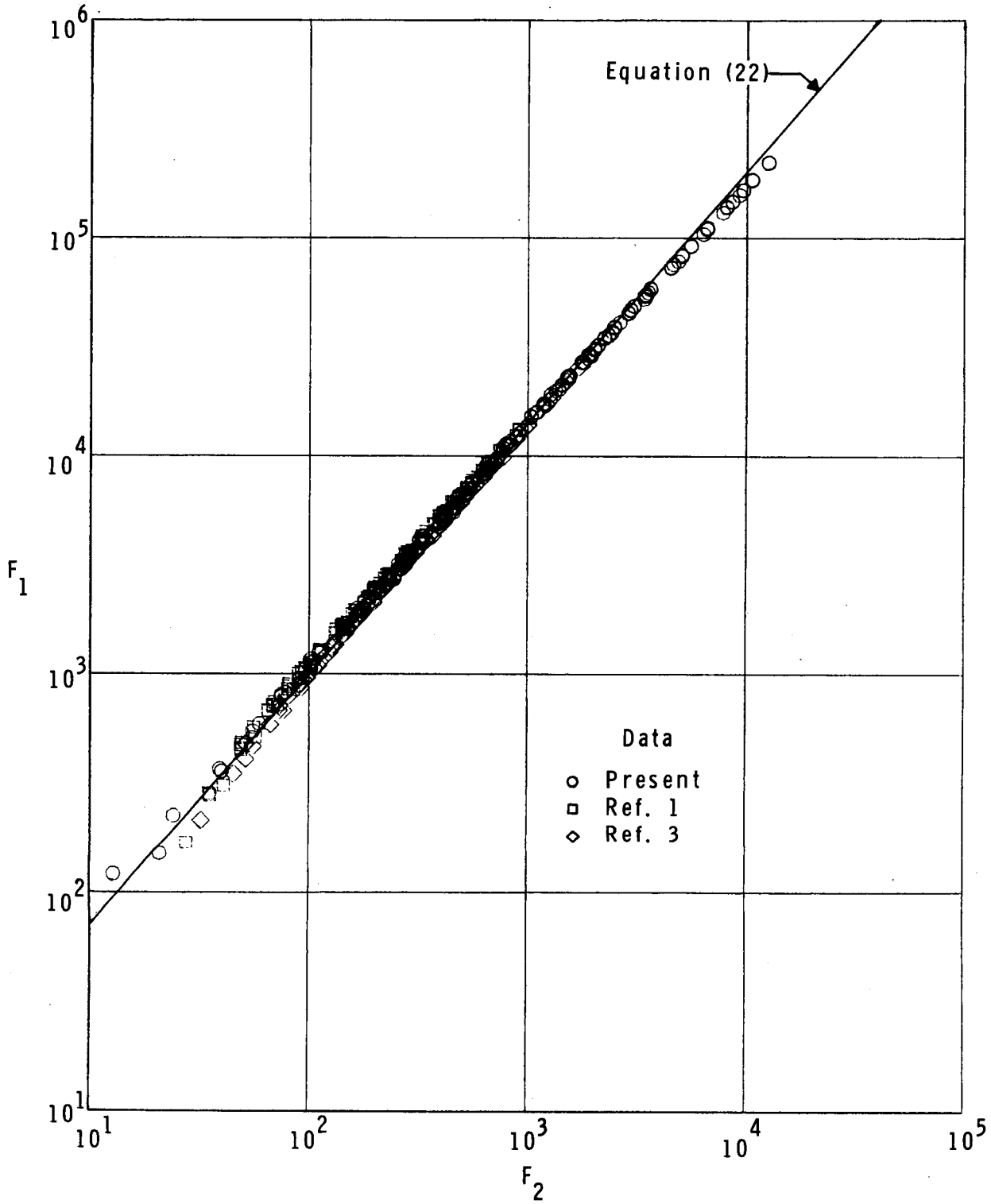

(a) Calibration parameters.

Figure 7.- Sigalla calibration equation.

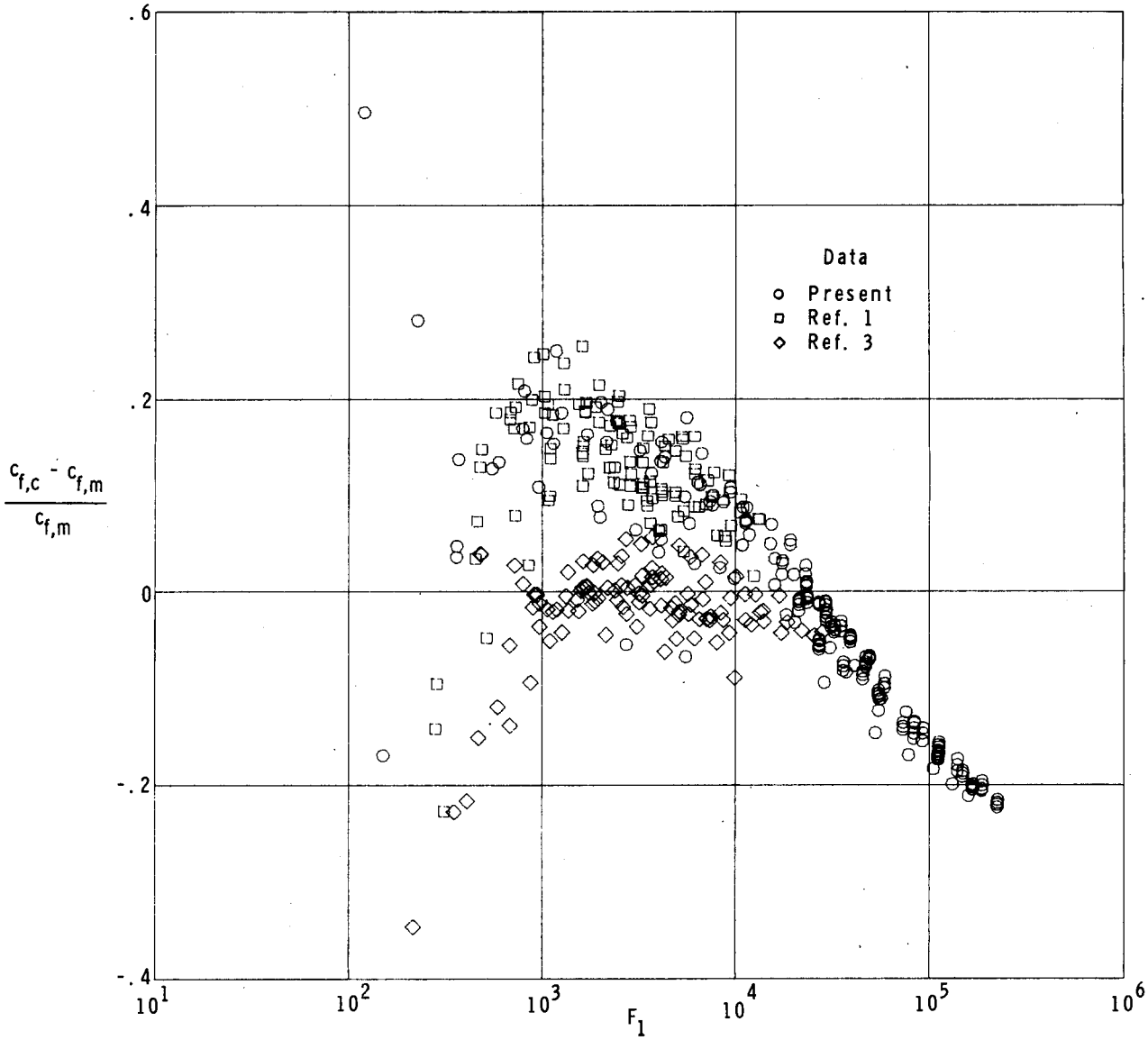

(b) c_f error.

Figure 7.- Concluded.

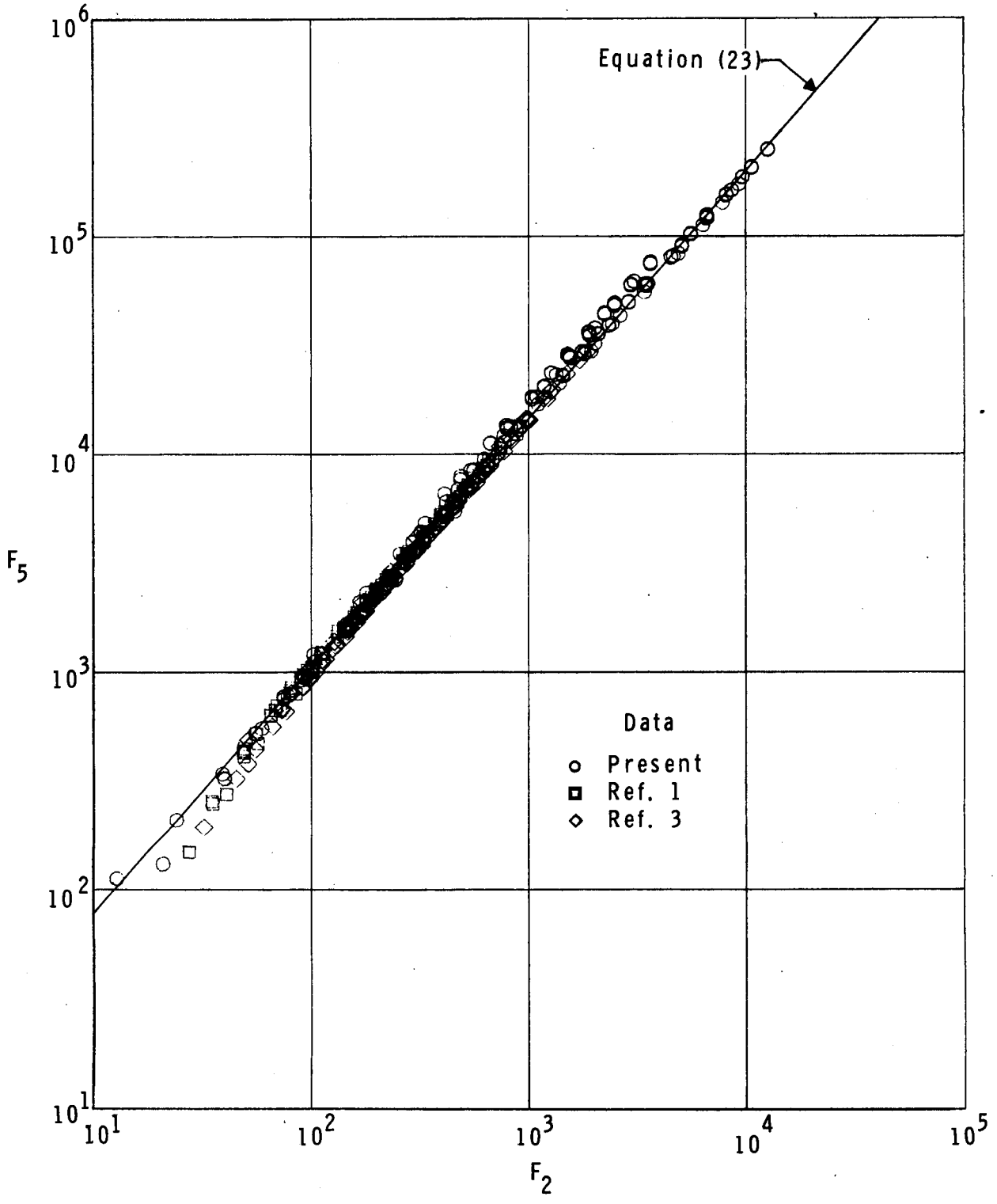

(a) Calibration parameters.

Figure 8.- Hopkins-Keener calibration equation.

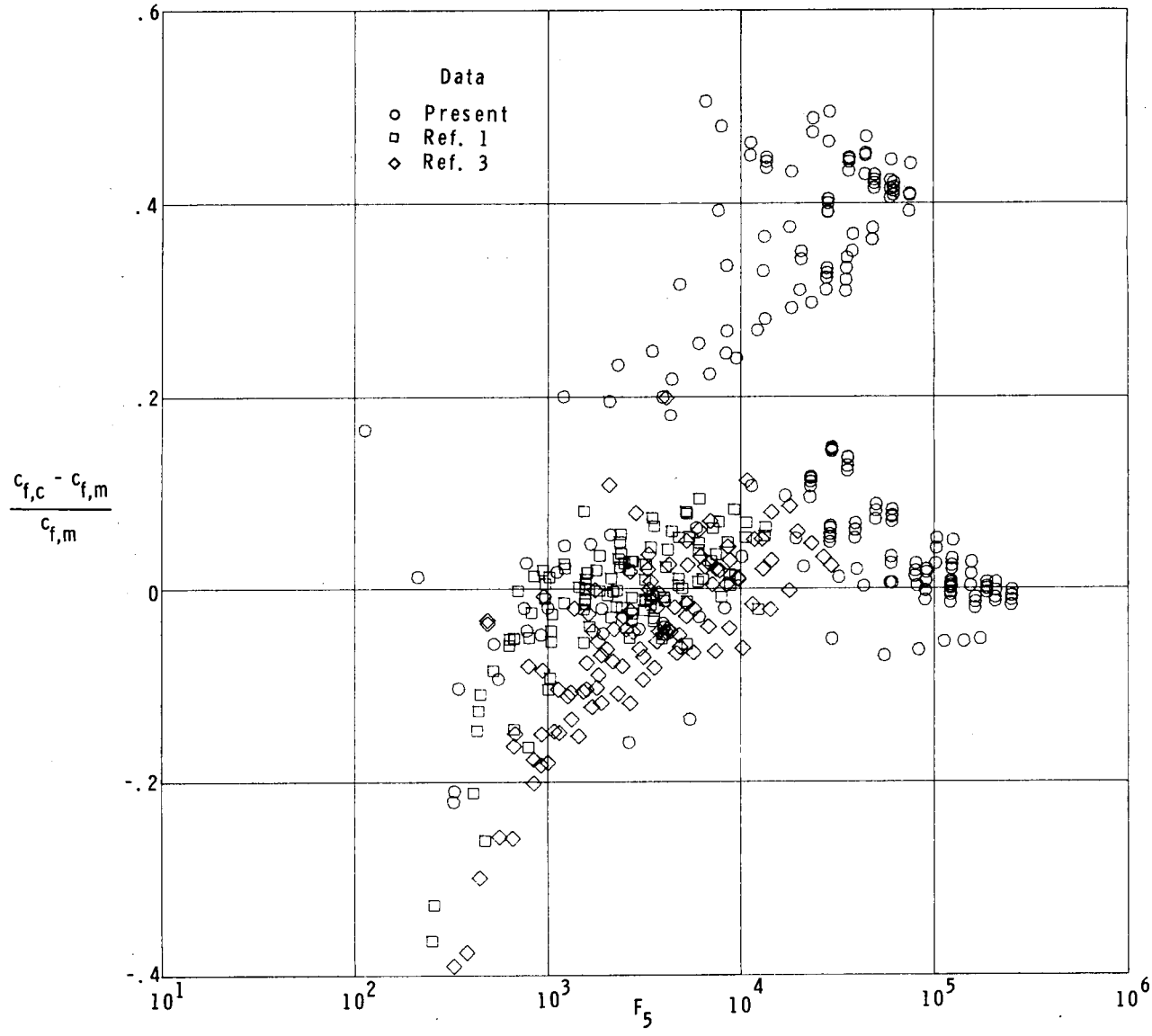

(b) c_f error.

Figure 8.- Concluded.

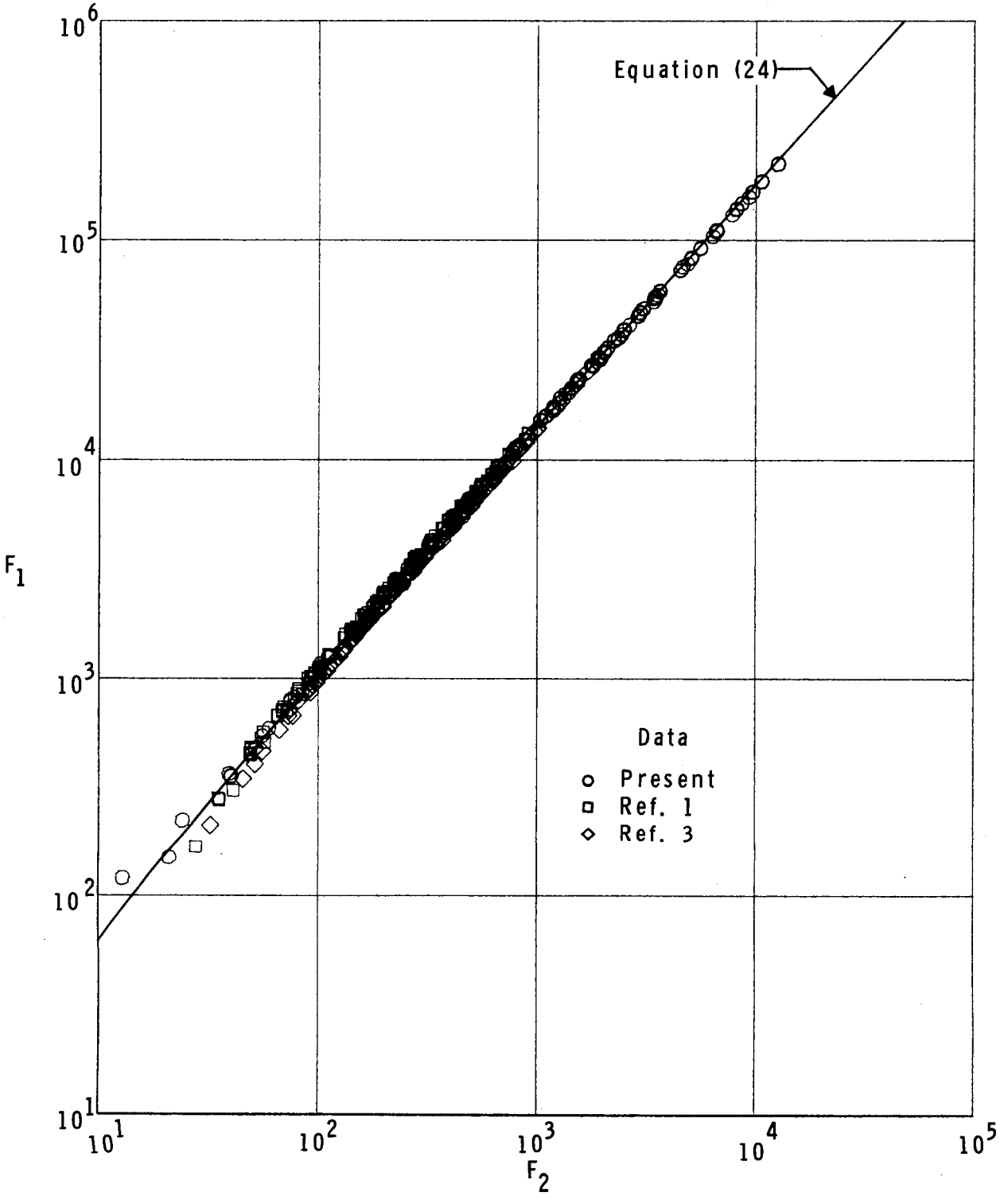

(a) Calibration parameters.

Figure 9.- Patel T' calibration equation.

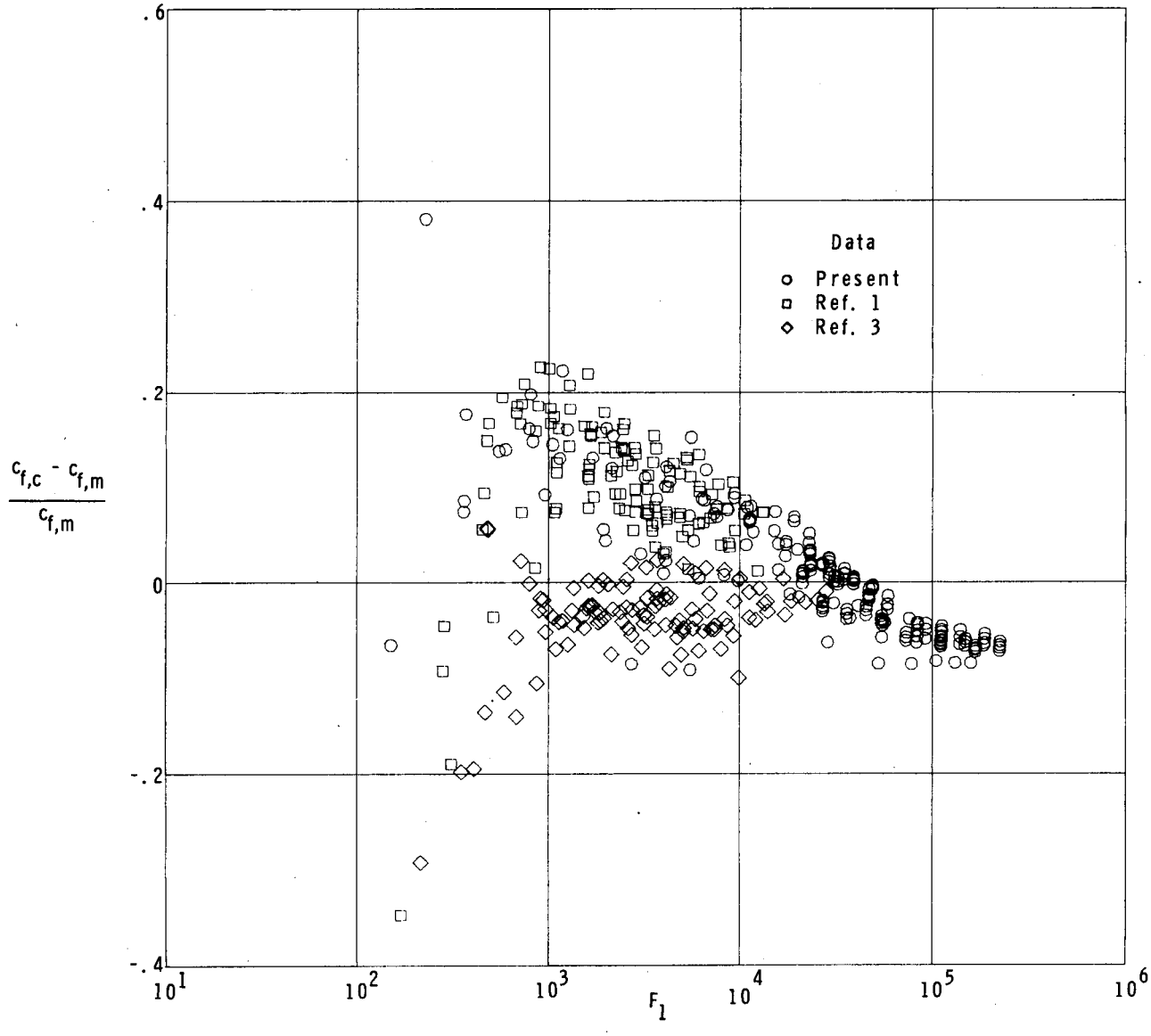

(b) c_f error.

Figure 9.- Concluded.

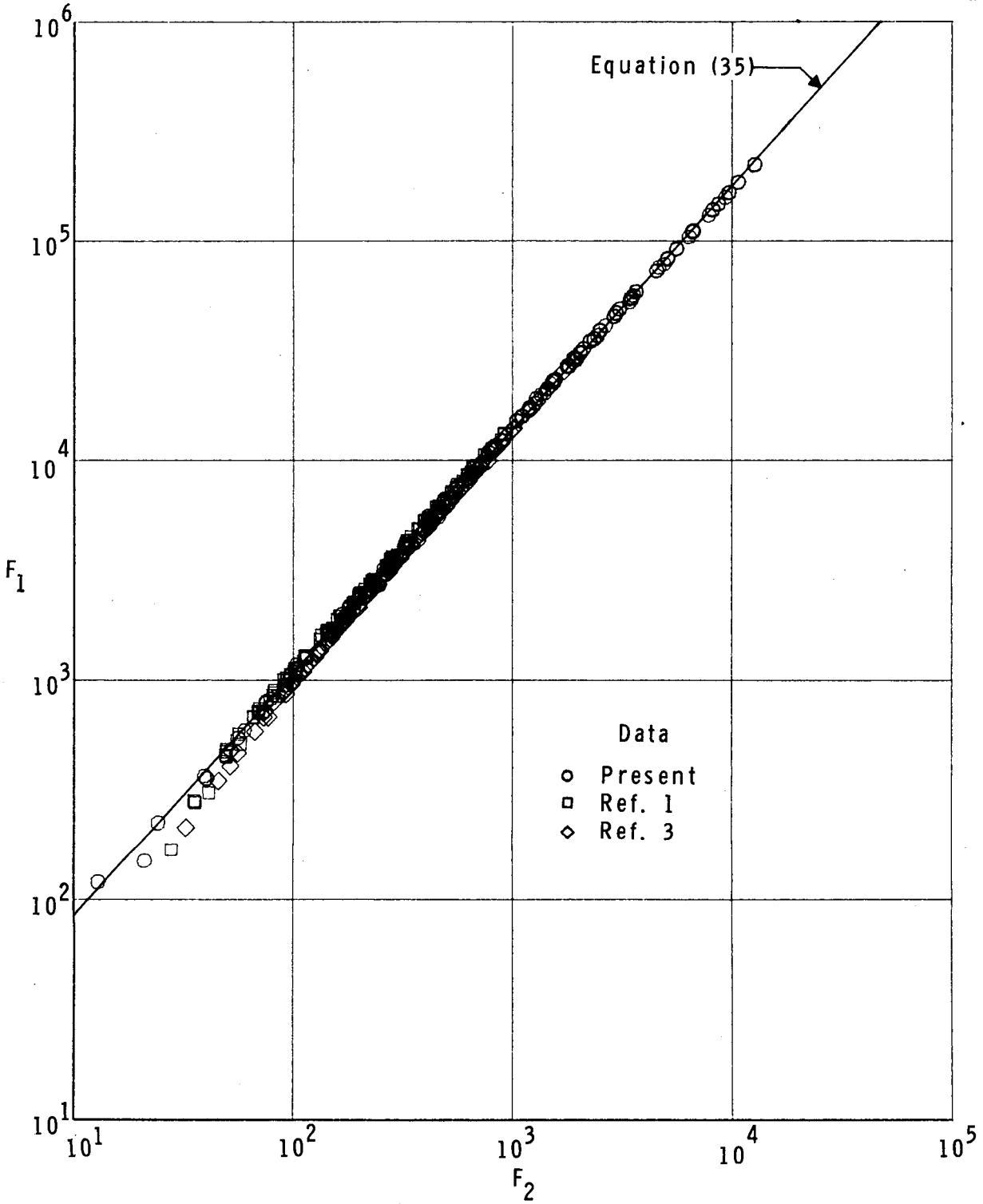

(a) Calibration parameters.

Figure 10.- Linear least-squares calibration equations.

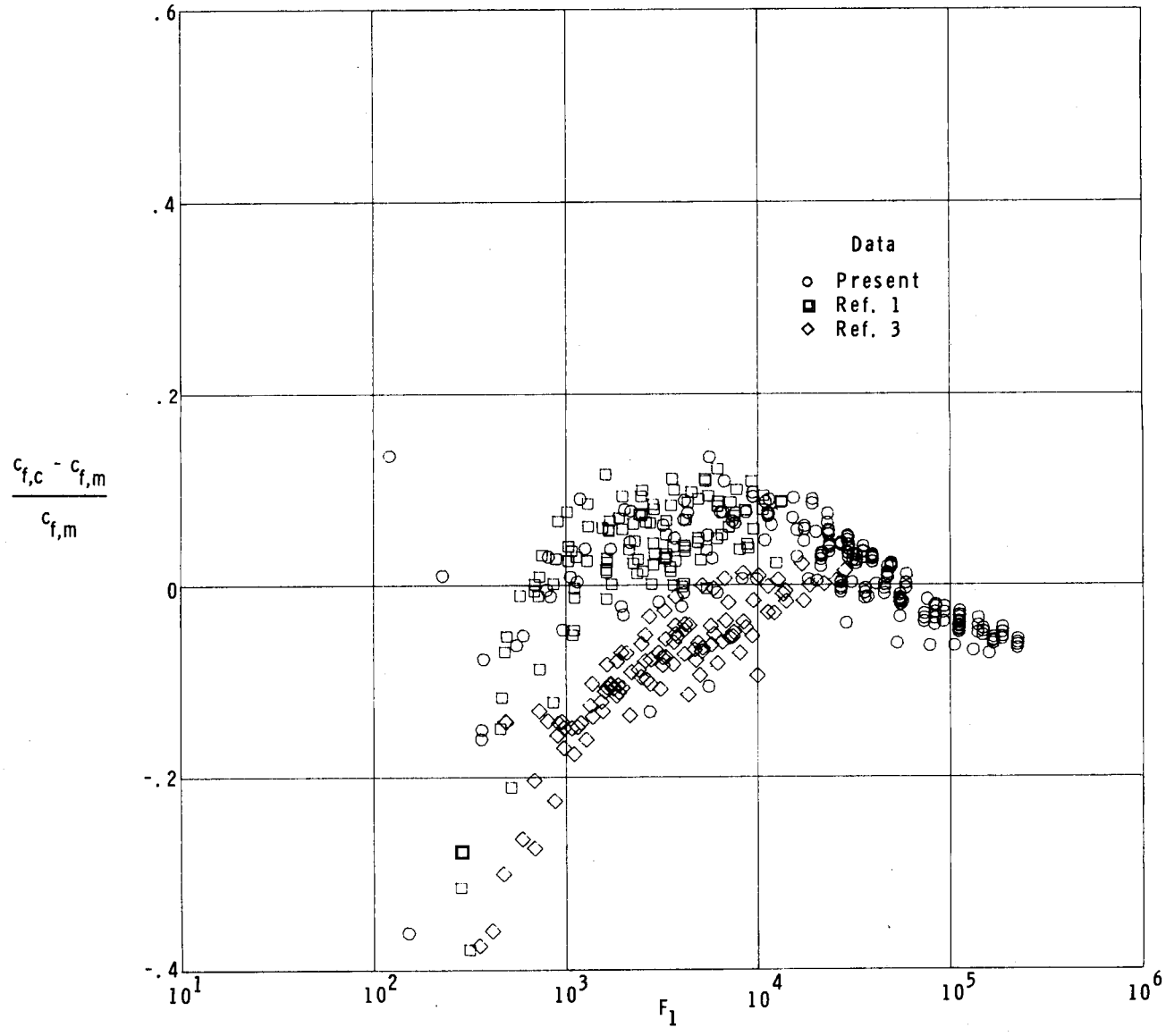

(b) c_f error.

Figure 10.- Concluded.

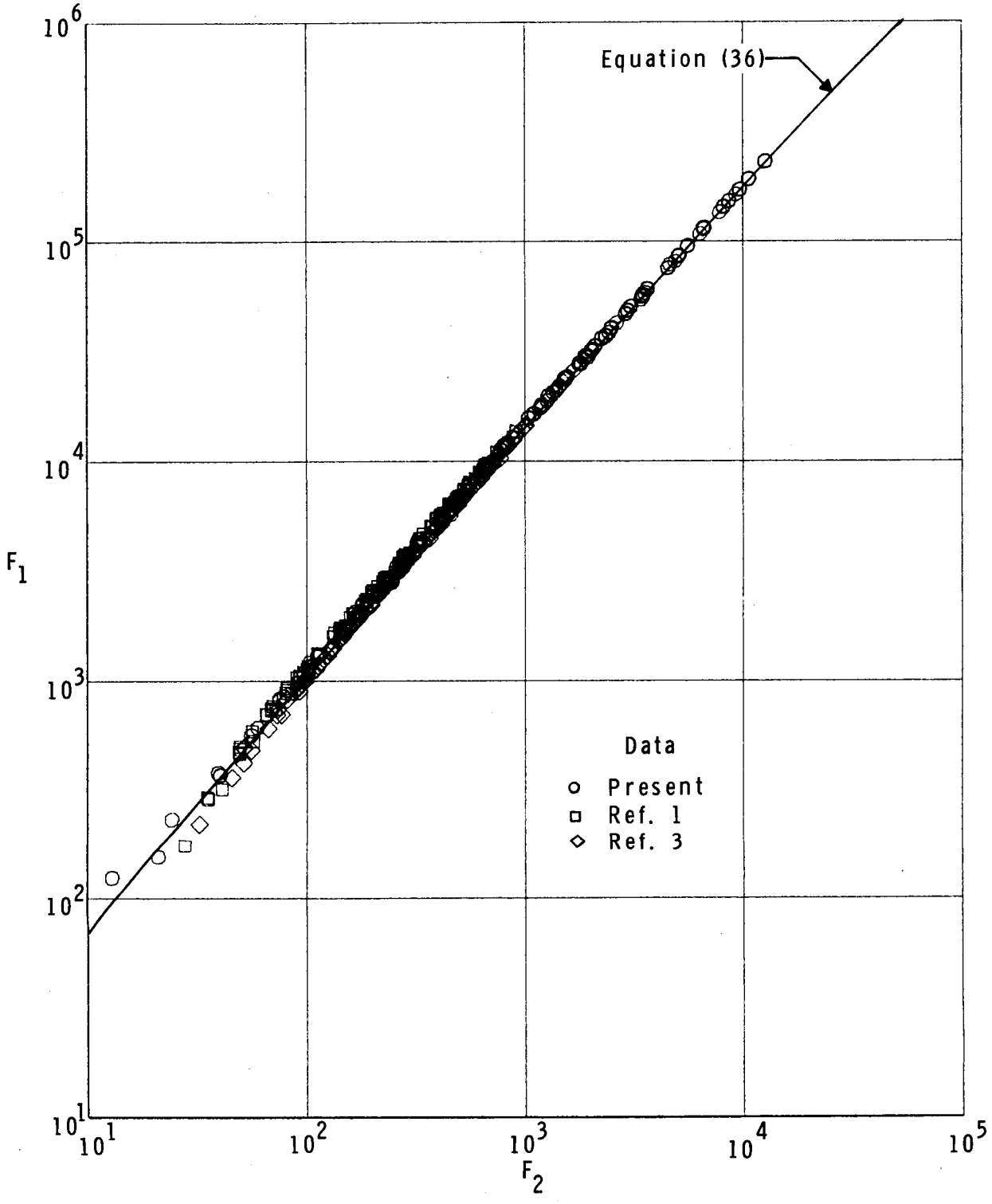

(a) Calibration parameters.

Figure 11.- Second-order least-squares calibration equation.

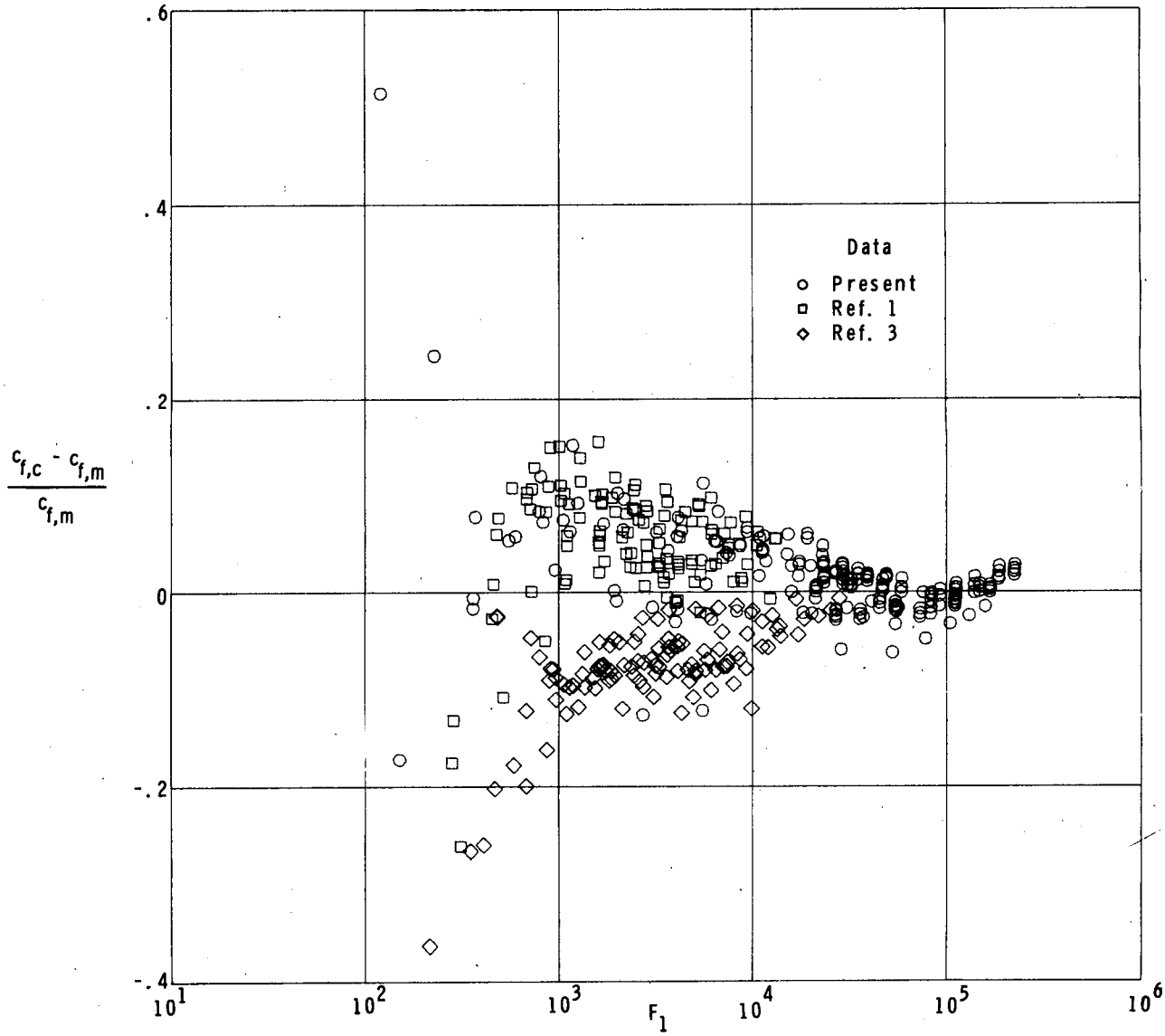

(b) c_f error.

Figure 11.- Concluded.

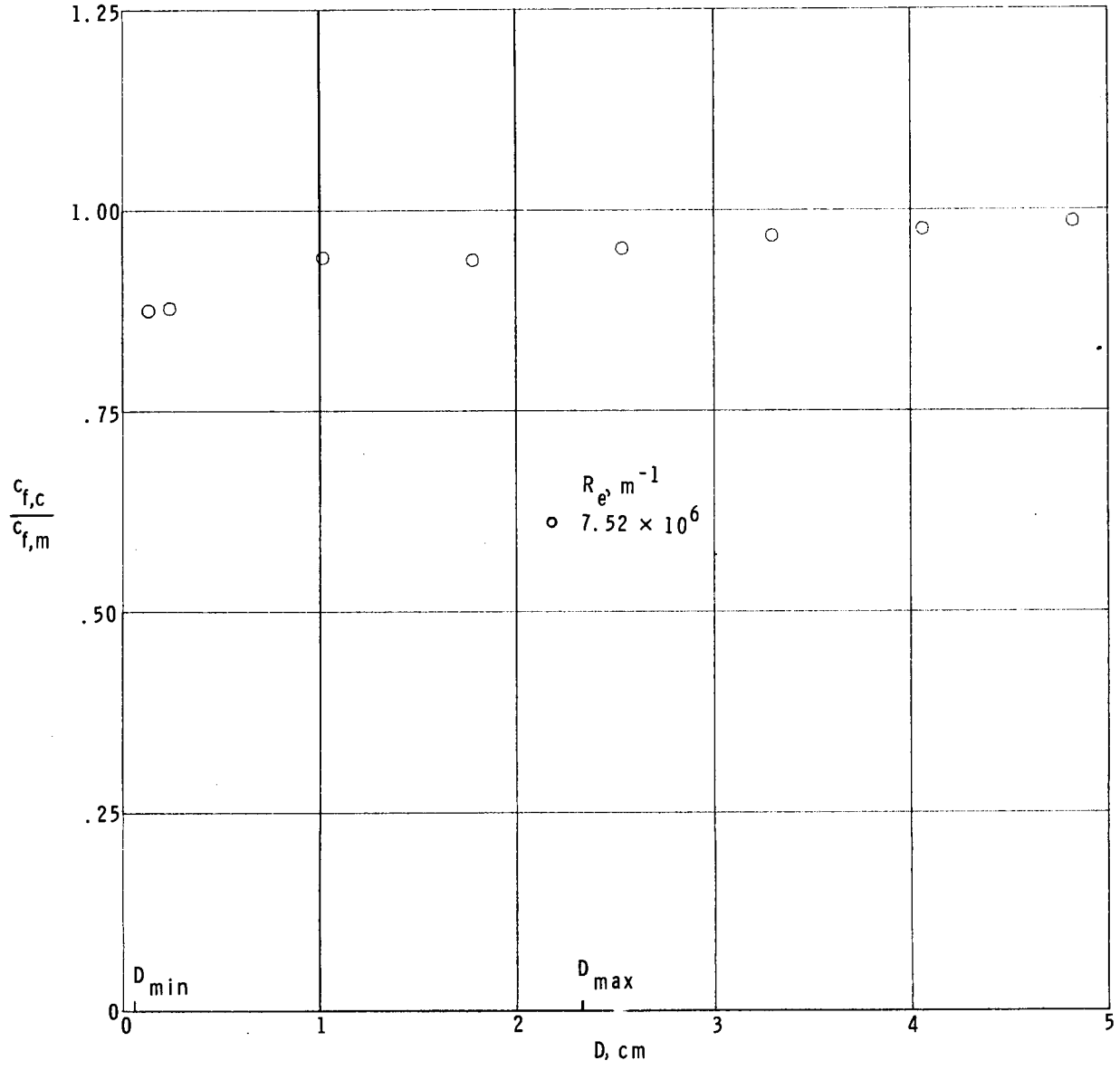

(a) $M_e = 1.975$.

Figure 12.- Effect of tube size on Preston tube skin friction.

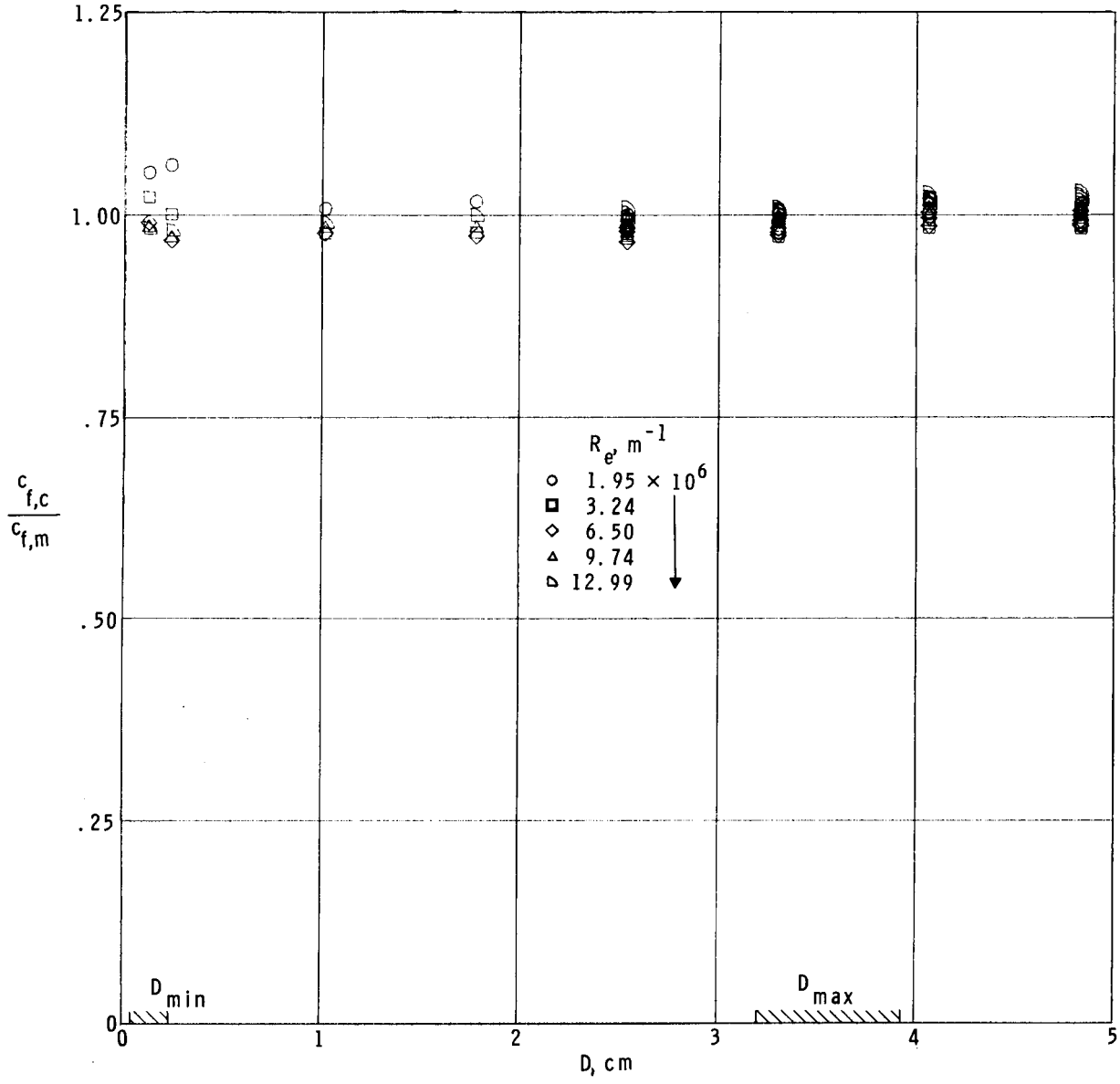

(b) $M_e = 2.320$.

Figure 12.- Continued.

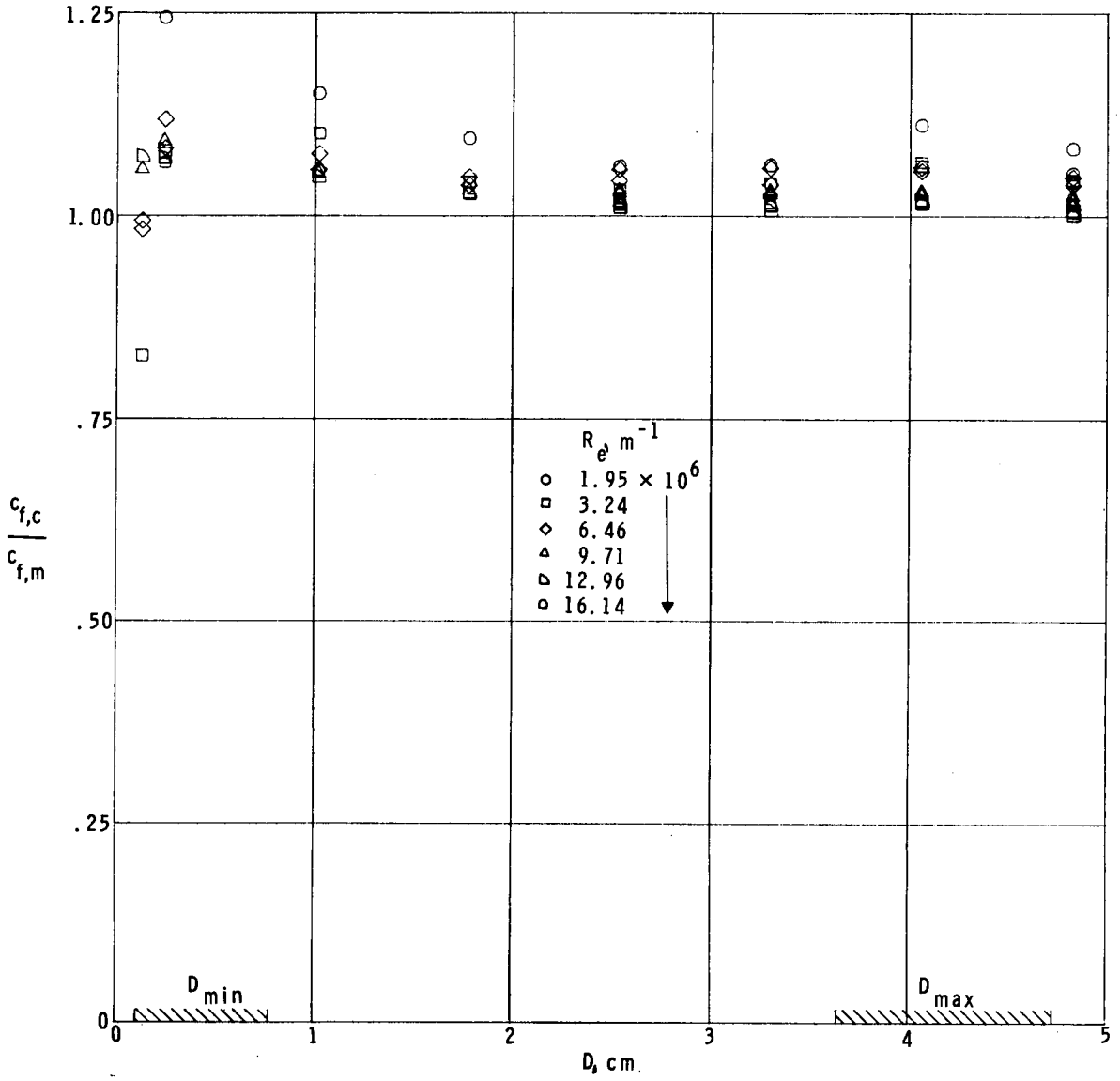

(c) $M_e = 4.630$.

Figure 12.- Concluded.

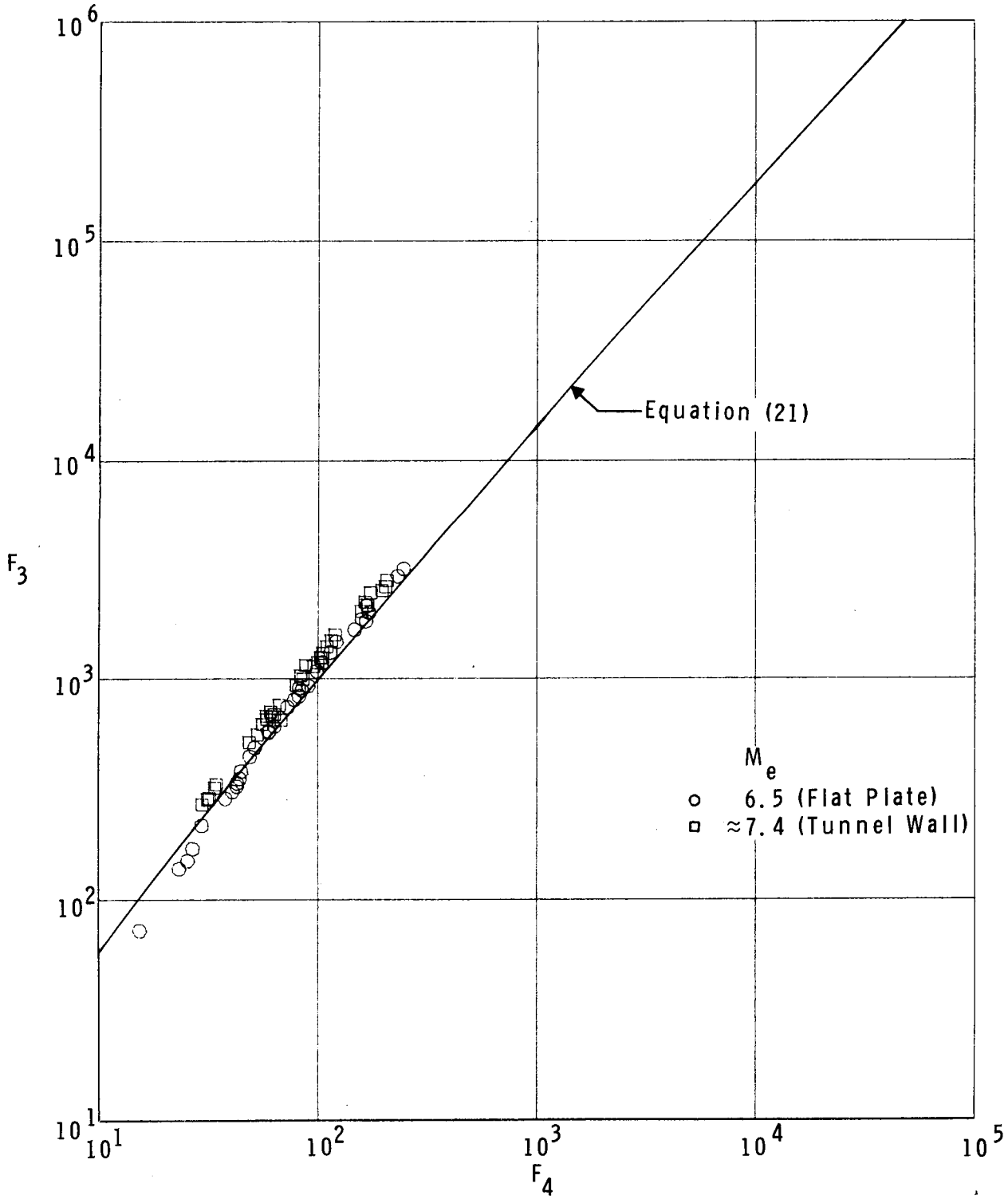

(a) Fenter-Stalmach equation.

Figure 13.- Comparison of calibration equations with hypersonic data of reference 7. $0.32 < T_w/T_{aw} < 0.51$.

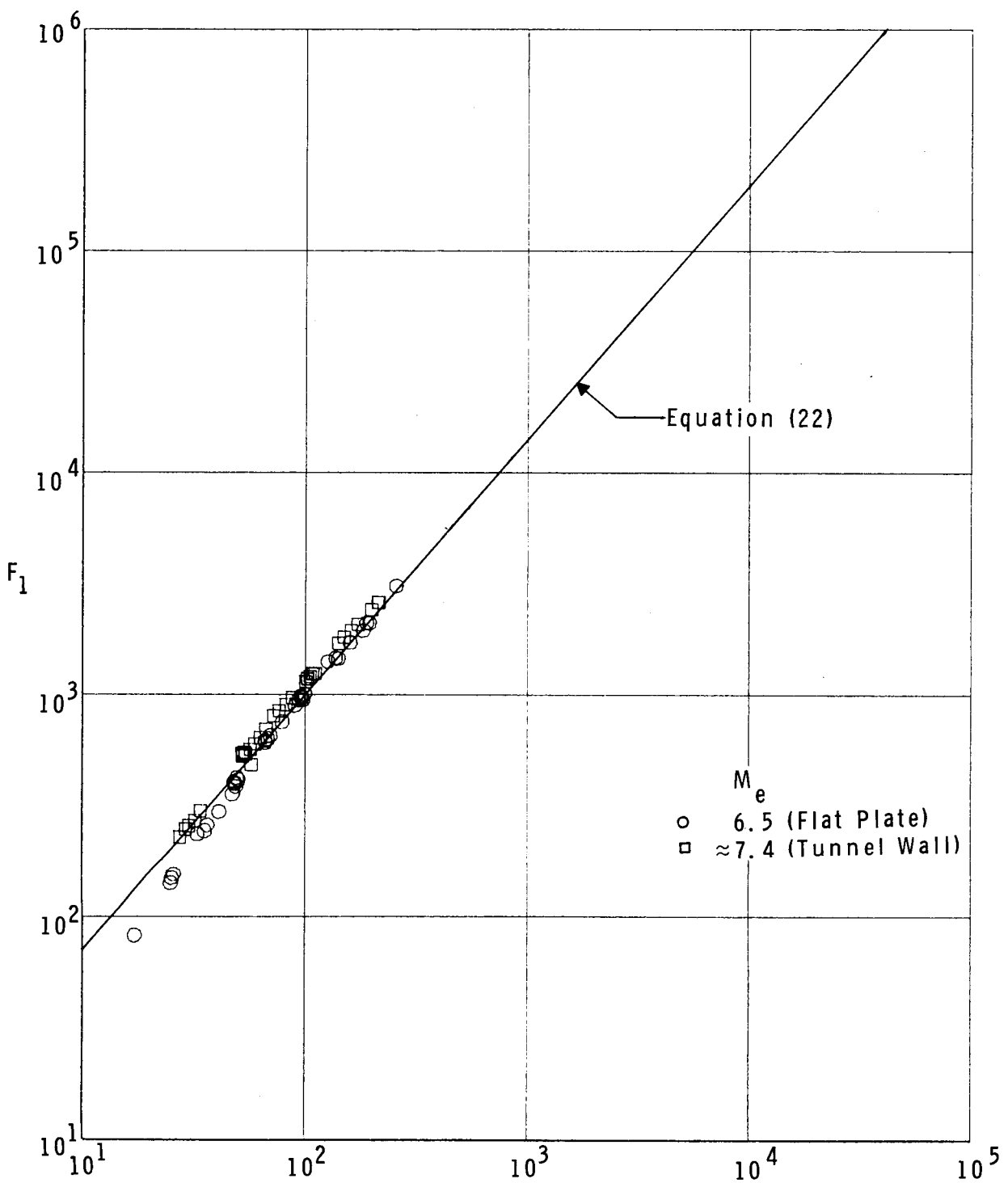

(b) Sigalla equation.

Figure 13.- Continued.

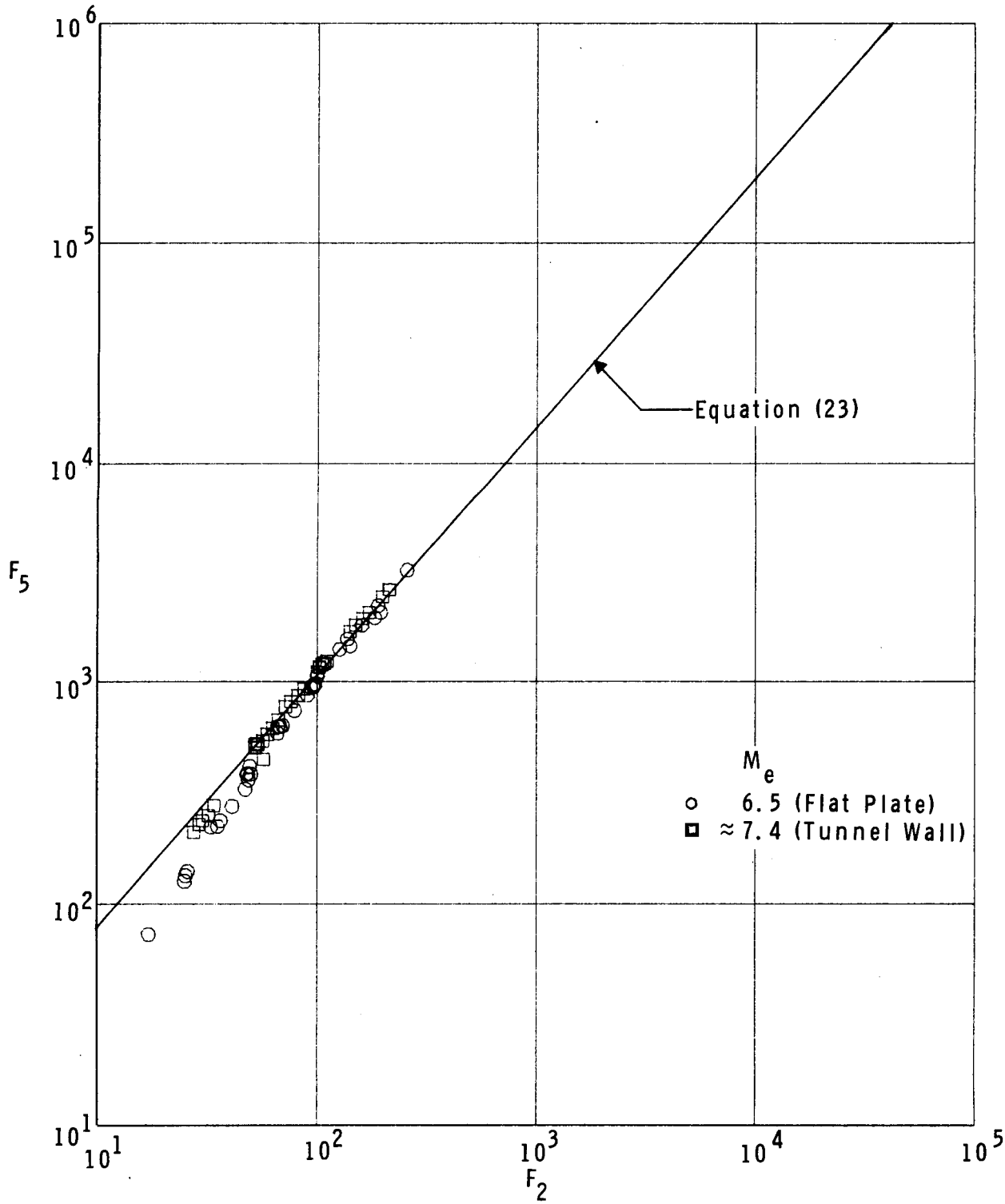

(c) Hopkins-Keener equation.

Figure 13.- Continued.

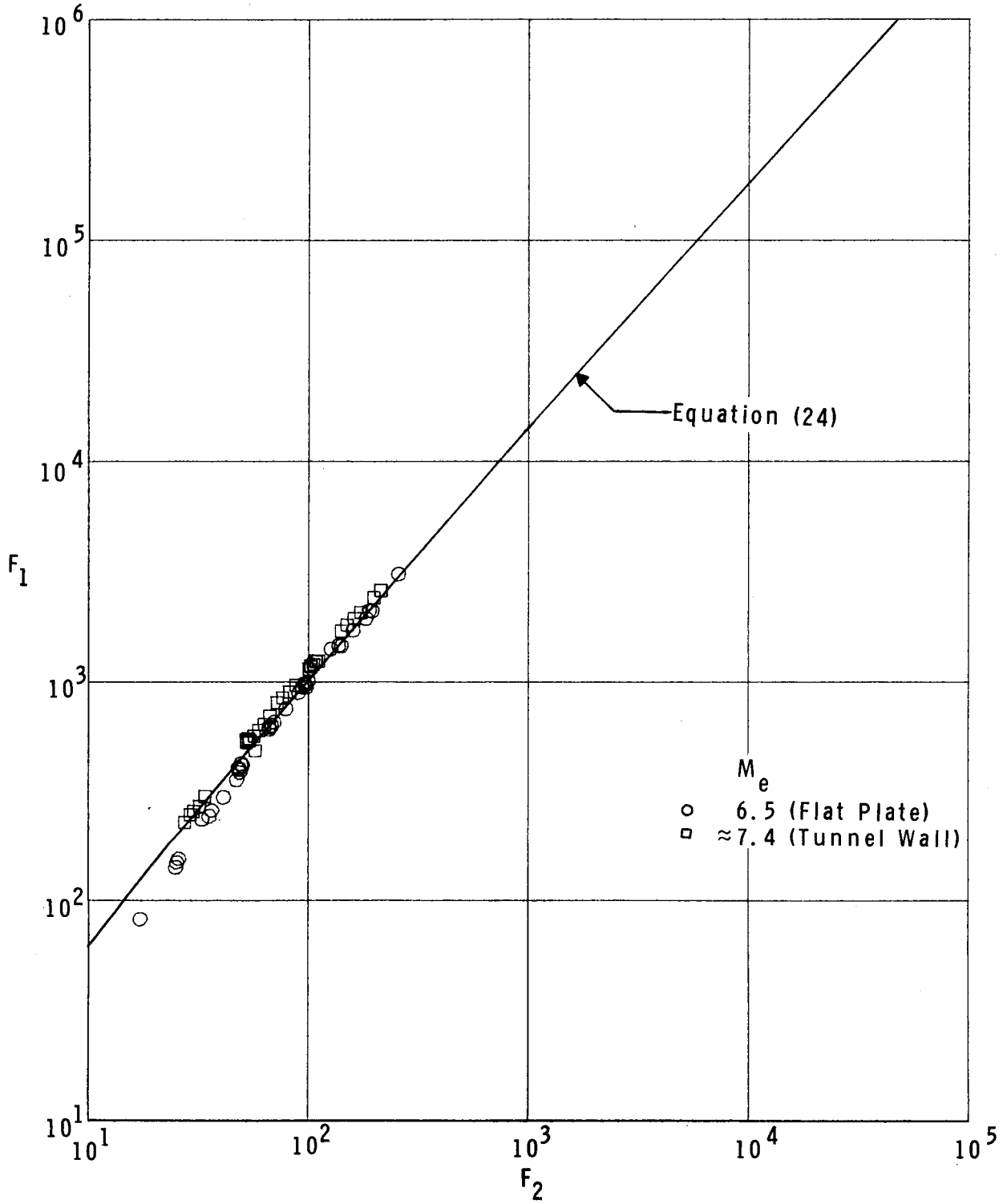

(d) Patel T' equation.

Figure 13.- Continued.

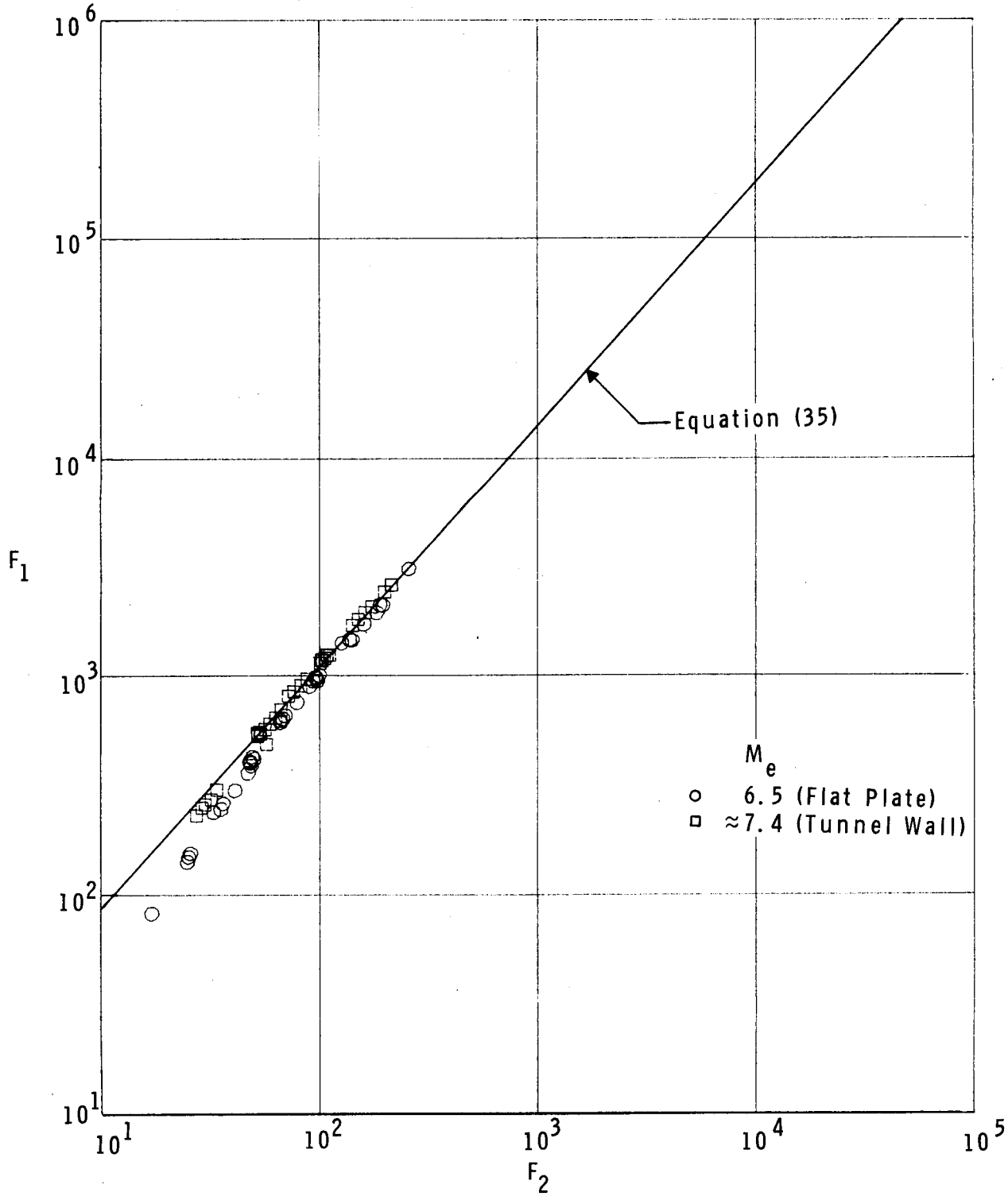

(e) Linear least-squares equation.

Figure 13.- Continued.

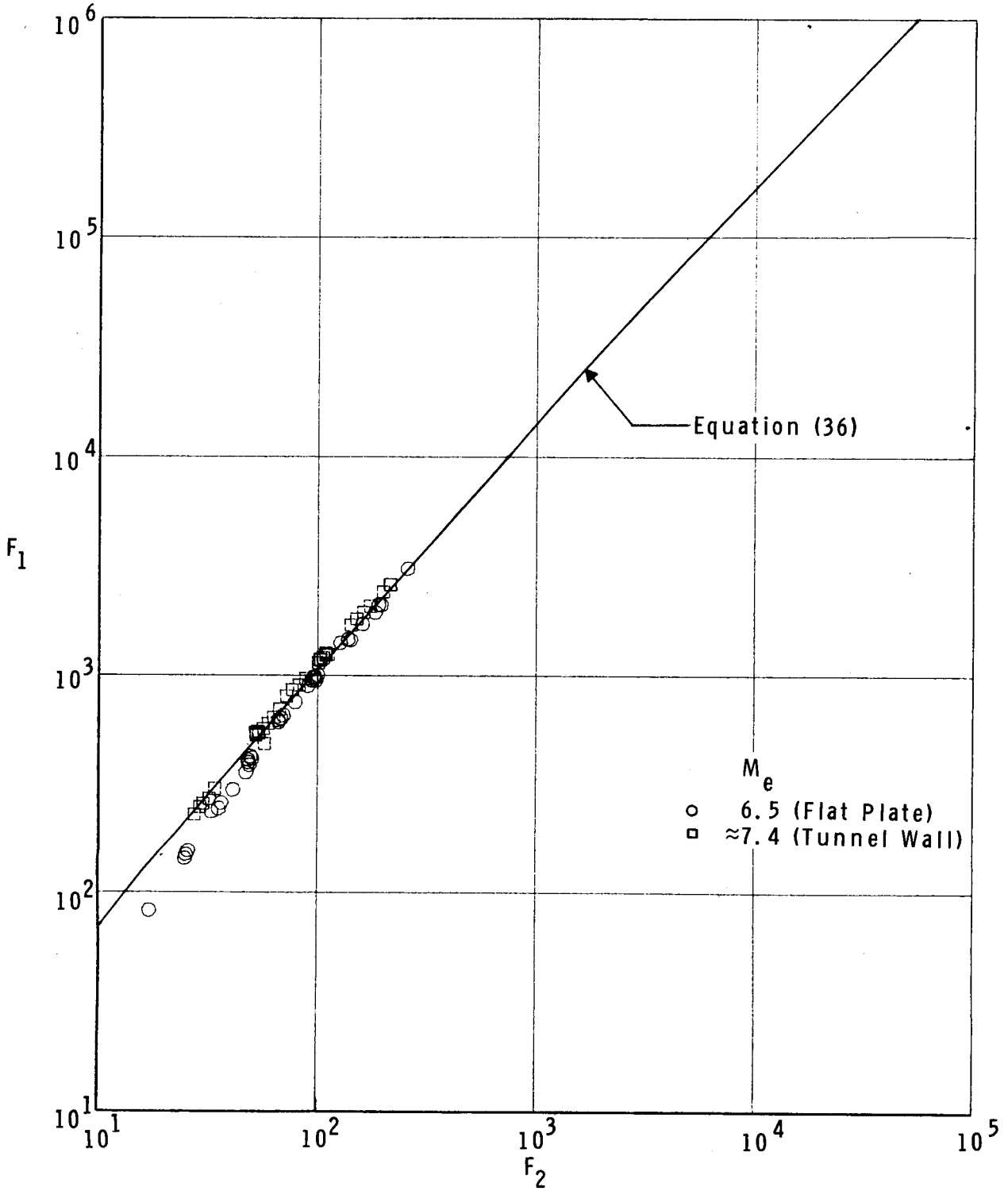

(f) Second-order least-squares equation.

Figure 13.- Concluded.